National Physical Laboratory

NPL REPORT MAT 103

FRACTURE AND CRACKING IN COATINGS

MARK GEE, TONY FRY, HELEN JONES, CAITLIN GREEN,
FREYA BOOTH-DOWNS, THOMAS ROACH

MARCH 2022

Department for
Business, Energy
& Industrial Strategy

FUNDED BY BEIS

Fracture and Cracking in Coatings

Mark Gee, Tony Fry, Helen Jones, Caitlin Green, Thomas Roach
Engineering Department

ABSTRACT

This report describes work that illustrates different microstructural characterisation approaches to the examination of fracture and cracking of coatings and engineered surfaces when subjected to mechanical loading. The methods that were used to apply the mechanical loading were sliding wear, scratch testing and Rockwell (Mercedes) indentation. Both optical and SEM based microscopy methods were used with a particular focus on 3D SEM-FIB as a way of assessing the sub-surface damage from deformation.

It was found that the use of both optical and SEM based techniques when combined with other measurements about the response of the materials such as friction and overall deformation gave a better understanding of behaviour. 3D-FIB revealed some very complex behaviour for the failure of coated and surface engineered materials when scratched.

ISSN: 1754-2979

https://doi.org/10.47120/npl.MAT103

National Physical Laboratory
Hampton Road, Teddington, Middlesex, TW11 0LW

This work was funded by the UK Government's Department for Business, Energy and Industrial Strategy (BEIS) through the UK's National Measurement System programmes.

Approved on behalf of NPLML by
Stefanos Giannis
Science Area Leader Advanced Engineered Materials

CONTENTS

1 FAILURE OF COATINGS FROM FRACTURE

Coating the surfaces of components has become an important route to improve the performance of products giving major improvements in their durability and lifetimes [1]. There are also materials such as tool materials that have been engineered specifically to have excellent surface performance.

One of the failure mechanisms that can occur for coatings and engineered surfaces is fracture and cracking from mechanical overloading in applications. This report discusses how the observation of fracture and cracking in these situations can be used to develop an understanding of how the functionality of the coating or engineered surfaces can be improved.

2 METHODOLOGY

2.1 MATERIALS

Several different materials which had engineered surfaces were examined as shown in Table 1. There was one hardmetal tool material, and 3 ASP23 tool steel samples that had been coated with different coatings. The test balls for the sliding wear tests were Si_3N_4 bearing balls.

Table 1: Materials

Name	Composition	Hardness	Thickness (for coating)
mars11E	Monolithic hardmetal with 11% cobalt remainder WC, 4 µm grain size	10 GPa	-
Nitron	Nitron coating on ASP23 hardened tool steel. Two layer composite of carbon on titanium	Substrate hardness of 66 HRC, Nitron hardness 12 GPa	3 µm
TiN	TiN coated ASP23 hardened tool steel	Substrate hardness of 66 HRC, TiN hardness 23 GPa	3 µm
WC/Co coating	Thermally sprayed WC/Co coating on ASP23 hardened tool steel substrate	Substrate hardness of 66 HRC, WC/Co hardness of 12 GPa	150 µm
Balls	Si_3N_4	Hardness 16 GPa	-

Cross sections were made across the coatings and polished then examined in an optical microscope and scanning electron microscope combined with energy dispersive analysis to confirm the makeup of the coatings (Figure 1). Whereas the Nitron coating was found to be a composite with an interface layer of titanium and a top layer of carbon (Figure 1a), the TiN coating was confirmed to be a single layer coating (Figure 1b). The much thicker WC/Co coating had globular grains of WC embedded in a cobalt matrix (Figure 1c). Some porosity was visible in the coating.

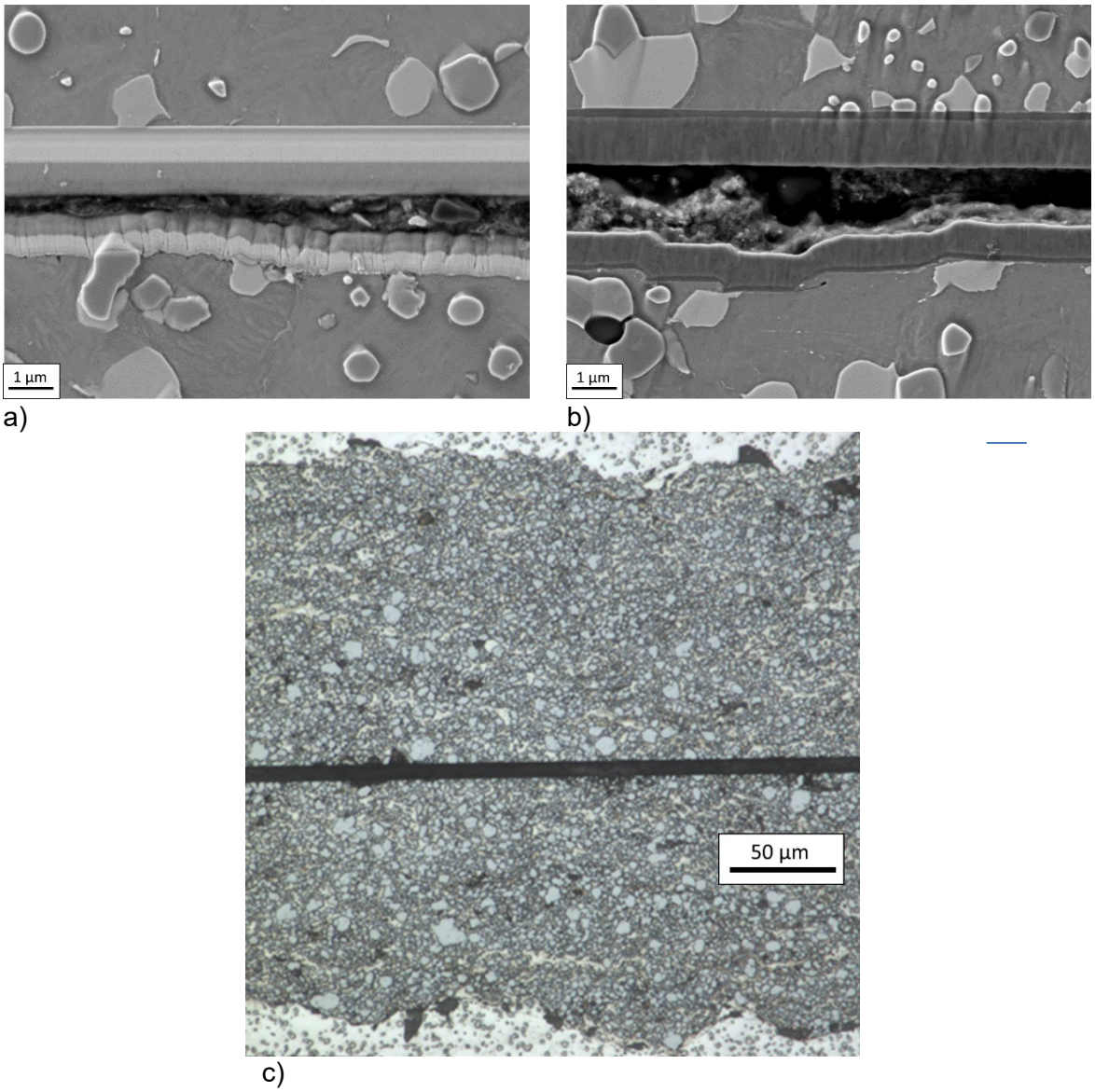

a) b)

c)

Figure 1: Cross sections through coatings, a) SEM of Nitron coating, b) SEM of TiN coating, c) Optical micrograph of WC/Co coatings. In all the images two samples were mounted back-to-back to retain the edge of the coating. In images a) and b) the lower sample shows the back face of the sample which has a rough surface.

2.2 TESTING

2.2.1 Sliding Wear

Pin-on disc wear tests were carried out with silicon nitride balls worn against the Nitron, TiN and WC/Co coatings (Figure 2). The tests were carried out with a pin on disc test system which has the capability for *in situ* real time imaging and topographical measurements of the wear surface and is also fitted with a self-zeroing friction measurement system for accurate measurement of friction (particularly important for low friction coatings such as DLC). A full description of the system and the results of the tests on the TiN and DLC coating are given in [2].

In the experiments that were carried out, changes in the visual appearance of the wear tracks and their topography were recorded and are available in [2].

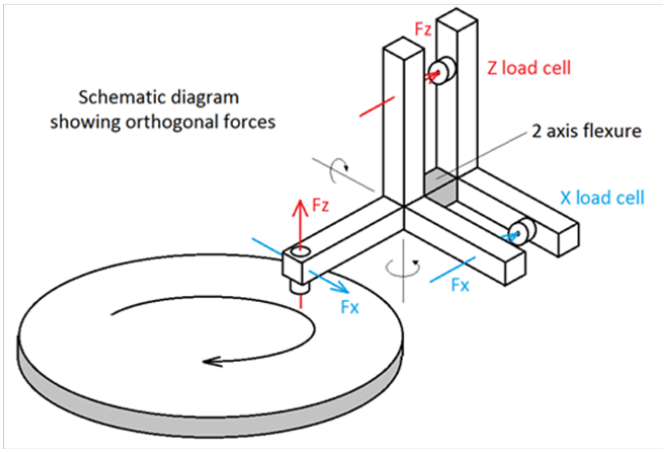

a)

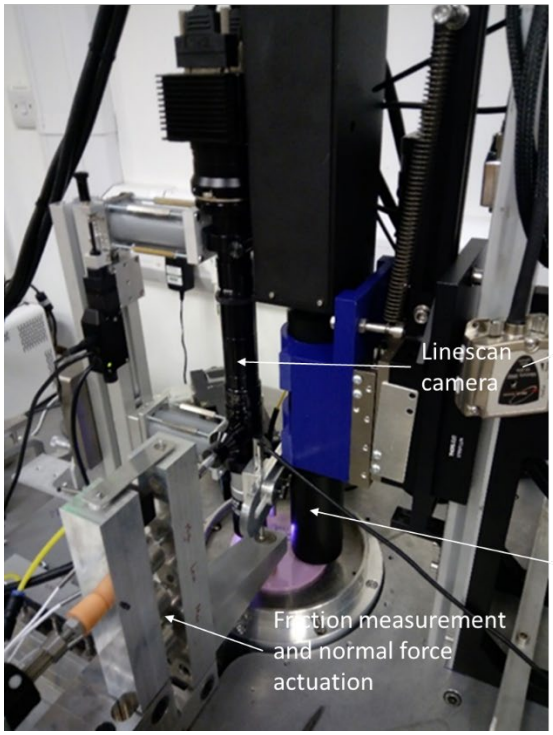

b)

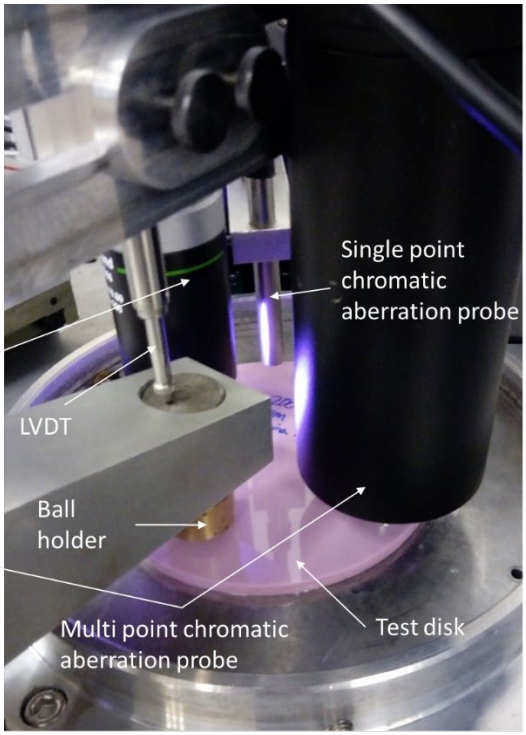

c)

Figure 2: Pin on disc test system, a) schematic of test system, global (b) and detailed (c) images showing the pin on disc test machine and the relative positions of the different components.

2.2.2 Rockwell

In the Rockwell adhesion test, a 200 µm radius diamond indenter is pressed into a coated surface (Figure 3). The substrate underlying the coating plastically deforms and lifts at the periphery of the indentation that is formed. The uplift in the substrate imposes tensile stresses into the coating and across the substrate-coating interface. These stresses can cause decohesion and cracking in the coating, and delamination and removal of the coating from the substrate. By making observations about the degree of cracking and delamination, the strength and adhesion of the coating is tested. This test is standardised in DIN and ISO [3,4].

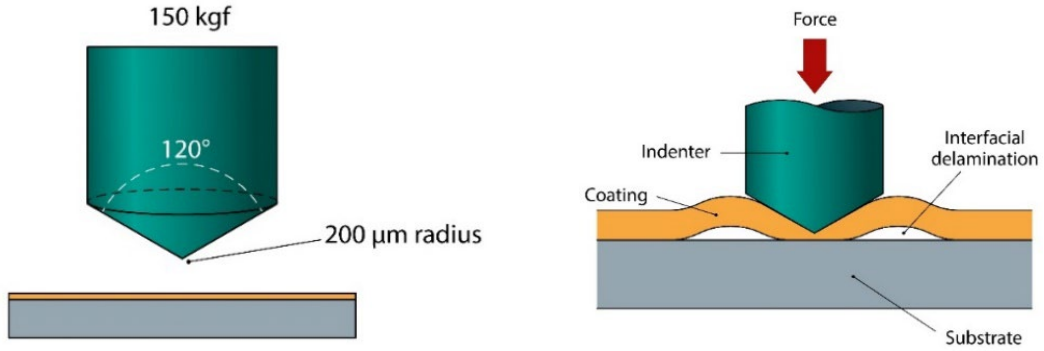

a) b)

Figure 4: Principle of Rockwell (Mercedes) test.

2.2.3 Scratch testing

The scratch test consists of pressing a diamond stylus onto the surface of the coating, using either a constant or an increasing load, whilst moving the sample at a constant speed (Figure 5). The test at constant load may be a single-pass scratch test or a multiple-pass scratch test. In the remainder of this report single pass increasing load scratch tests are used. There is a certified reference material, BCR-692, for use in this mode. The diamond stylus that is used is a 200 µm radius Rockwell C indenter. For further information see reference [5]. Figure 5 gives more information about the test. One of the goals of the test is to identify failure events and note the critical values Lc1,2,3 when these occur. Figure 5 also shows the identification of these events for the BCR-692 reference material.

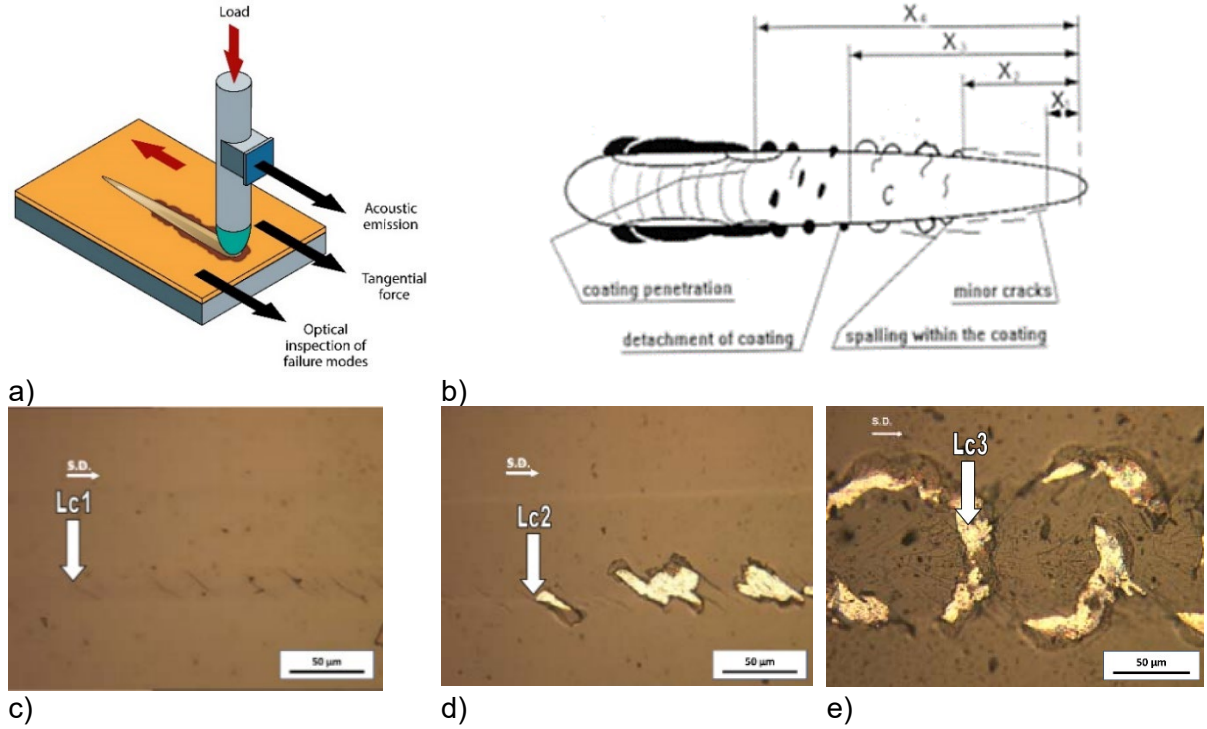

a) b)

c) d) e)

Figure 5: Scratch testing. a) Schematic diagram of scratch test system, b) schematic of failure events that can occur, c), d) and e) example of scratch events on carbon film BCR-692 scratch reference material c) Lc1 15N cracking, d) Lc2 20 N edge chipping, e) Lc3 30 N cross track chipping. S.D. is sliding direction

The identification of coating failure through cracking and fracture is normally carried out through optical microscopy of the scratch (Figures 5c-5e). This identifies critical loads Lc1,

Lc2, and Lc3. Lc1 is defined as the load at which the first cracking events associated with the scratch are detected. Lc2 is defined as the load where the first delamination events occur, and Lc3 is defined as the load at which complete delamination in the scratch occurs. The measurement of acoustic emission (sound generated at cracking events as fracture occurs) and tangential or friction force give additional information that can also give information on when critical transitions in behaviour occur (Figure 6).

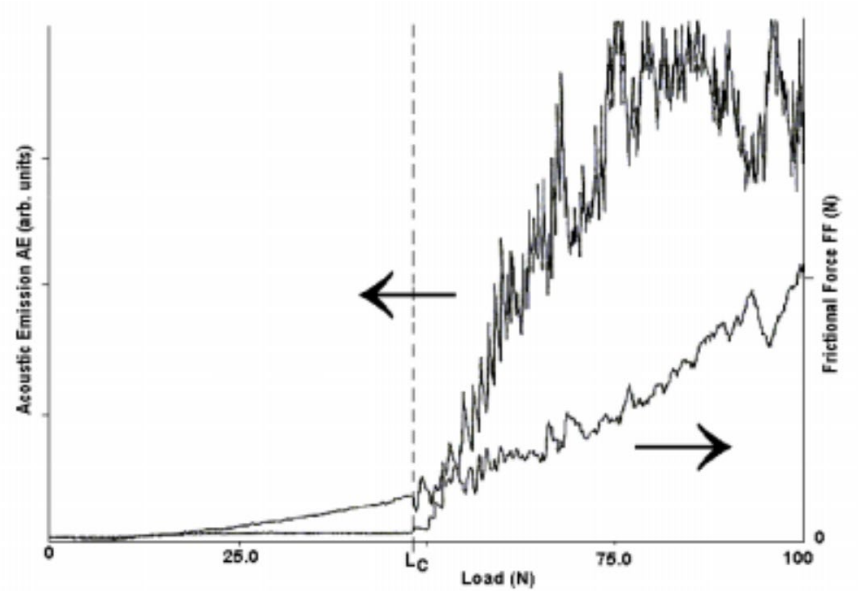

Figure 6: Typical trace for acoustic emission and friction force

2.2.4 Abrasion Simulation

As a simulation of abrasion, the 11E hardmetal sample was subjected to repeated scratching using the NPL microtribometer (Figure 7) as part of a larger study into computer controlled microtribology [6]. A 20 μm radius diamond indenter was pressed into the polished surface of the 11E sample and 200 repeat scratches were carried out with the same crack path.

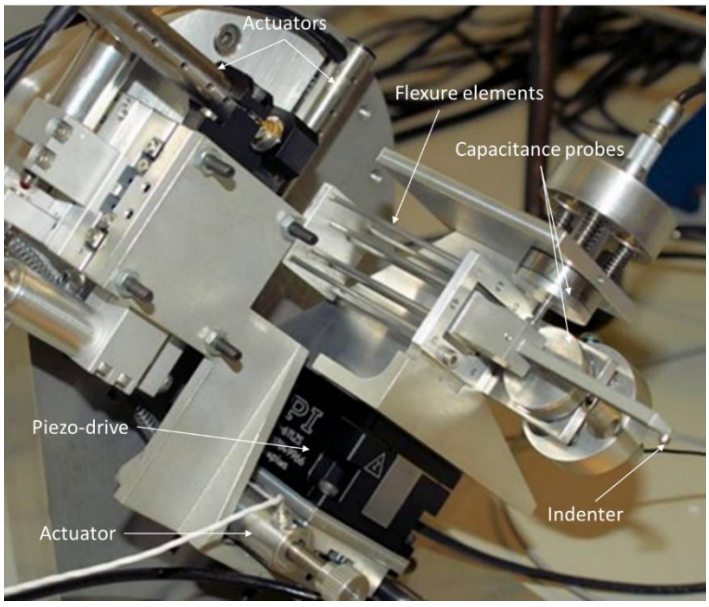

Figure 7: NPL micro-tribometer.

2.3 IMAGING FRACTURE AND CRACKING DAMAGE

Optical imaging of the damage caused by the mechanical overloading was carried out either with a Nikon measurement microscope, or with an Alicona G5 3D optical microscope. SEM imaging was carried out by a Zeiss Supra SEM or a Zeiss Auriga dual beam instrument which also provided 3D data sets where sequential images of slices machined away from the sample using the instruments gallium ion probe were acquired. Further information on 3D imaging using this FIB process is given in [7]. Post processing of these 3D data sets was carried out using the Image J image processing package.

3 FRACTURE SEEN IN DIFFERENT OVERLOADING SITUATIONS

3.1 SLIDING WEAR

Figure 8 shows some overall results from the *in situ* real time ball on disc tests. The normal applied load for the Nitron test was stepped in the early stages of the test (Figure 8a). At each load step there was a transient in the friction coefficient, but which did not affect the overall trend in friction. The effect of the changes in load can also be seen in the overall Linear Variable Differential Transformer (LVDT) wear displacement. At about 1040 rotations (passes) there is a much larger transient in the friction which leads to a permanent change in the friction coefficient trend. This is also seen in the averaged linescan information where there is a dramatic change in contrast. There are other transients in the friction throughout the remainder of the test which are also associated with changes in the averaged linescan image.

The normal applied load for the TiN test was kept constant at 50 N (Figure 8b). The friction coefficient in this test increases gradually throughout the test from 0.4 to 0.9. The averaged linescan information shows that the width of the wear track increases throughout this test.

Figure 9 (Videos in supplementary information) shows the *in situ* results from the *in situ* real time ball on disc test on the Nitron sample. At the start of the test, damage to the surface takes place quite slowly so that even after about 500 rotations of the disc only quite shallow score marks are shown on the wear track which have a depth of about 0.2 μm. As the test proceeds the width and depth of the damage increases (Figures 9c and d) until at 1046 rotations a substantial portion of the central region of the coating in the wear track is dramatically removed (Figures 9e and f). At the end of the test the coating across the whole width of the wear track has been removed (Figures 9g and h).

The post-test examination of the wear track confirmed this observation showing that the wear track on the disc was very scored, with a maximum depth of about 3 μm which was the original thickness of the coating (Figures 10a and c). The wear scar on the ball was quite flat and was circular, indicating that more wear had taken place to the ball than to the disc. The ball scar was also scored, with the pattern of scoring similar to the pattern of scoring on the wear track on the disc. A small amount of debris had built up at the leading edge of the ball scar (Figures 10b and d). (Note that another version of Figure 10 is in the supplementary information with 3D height plots of the wear track and the ball)

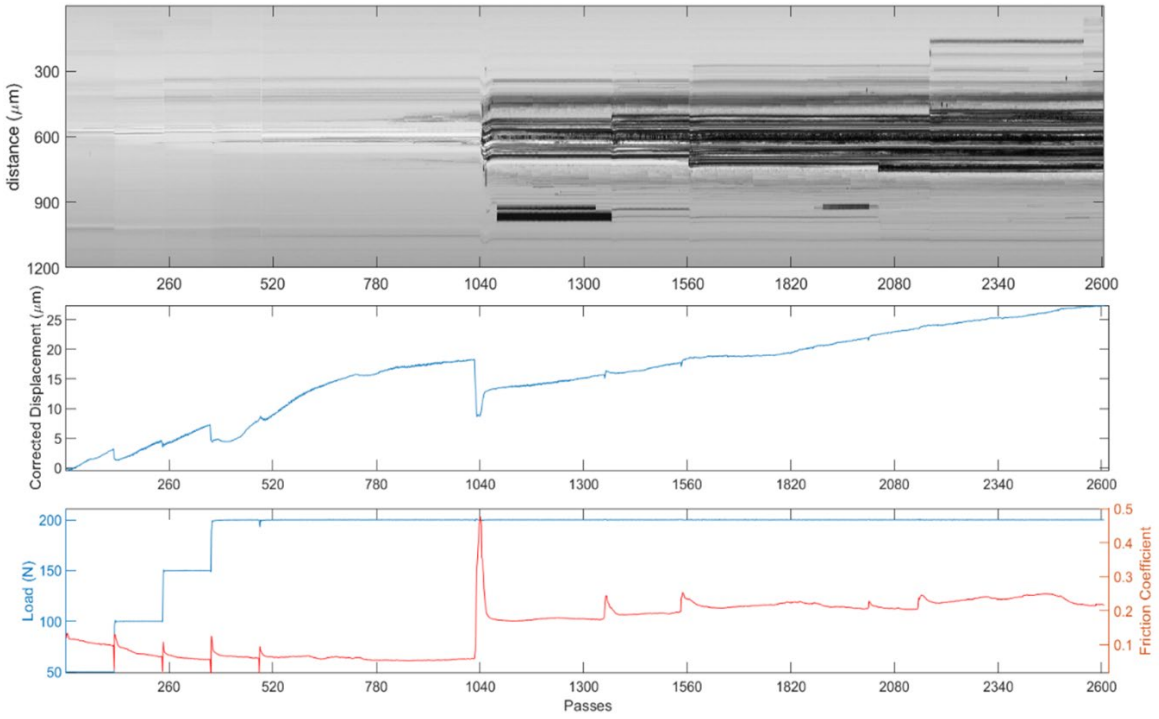

a)

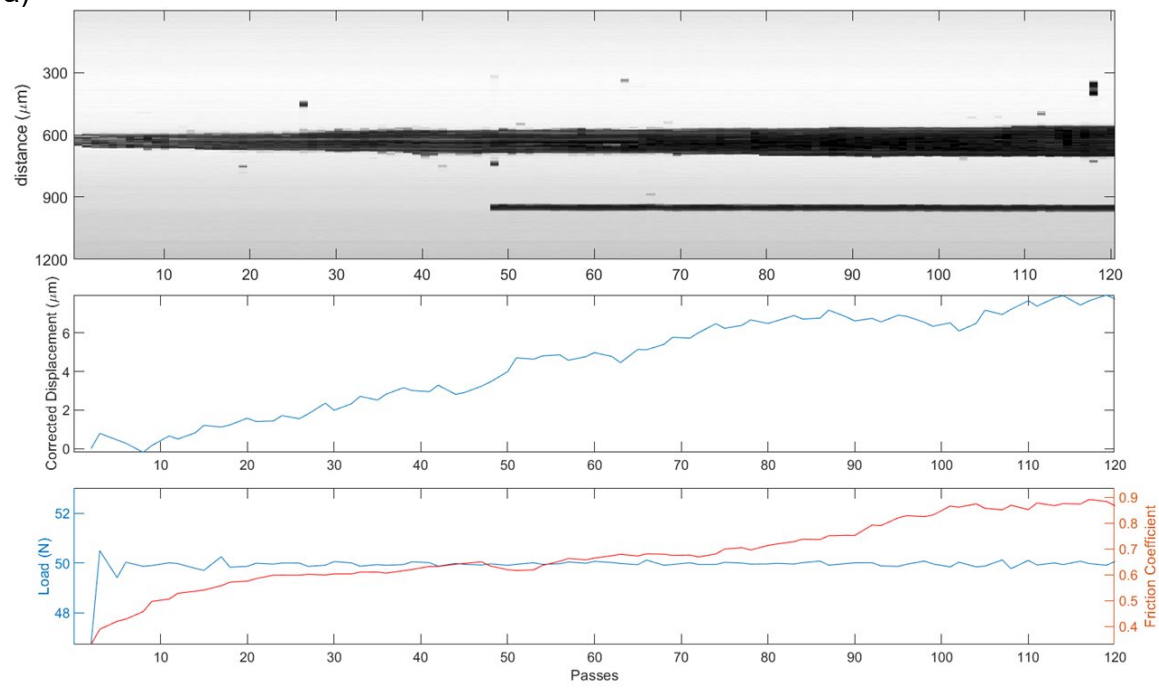

b)

Figure 8: Overall results for ball-on disc tests, a) averaged linescan information (top), overall LVDT displacement (middle) and load (blue) and friction coefficient (red) for Nitron coated disc, b) averaged linescan information (top), overall LVDT displacement (middle) and load (blue) and friction coefficient (red) for TiN coated disc. In the averaged linescan images each vertical line in the averaged image is an average of an entire linescan image. Thus the averaged image presented here gives a simple depiction of the entire time history of the visual image of the wear track.

The ball on disc results for the TiN test showed different results (Figure 11 and 12, Videos for Figure 11 in Supplementary information). Here, there was an increase in the damage to the disc from the start of the test until the end of the test without a sudden removal of the coating

from the area of the wear track. Initially, the wear to the disc removed material from the disc, but at about 80 rotations the height of the worn area increased through the transfer of material to the surface of the disc (Figures 11c and d). At the end of the test the wear track on the disc was again lower than the surrounding disc surface. This is also shown by the post-test surface examination where a clear groove is seen in the wear track (Figures 12a and c). The wear scar on the ball was again circular (Figures 12b and d), but there had been transfer of material to the ball which had had a thickness of about 10 µm, shown where a large fragment of this transfer layer had fractured and been removed from the worn surface. (Note that another version of Figure 12 is in the supplementary information with 3D height plots of the wear track and the ball)

Comparing the ball on disc tests for the two different coatings, in the ball on disc tests on the Nitron coated sample there was initially gradual removal of material from the coating by abrasion processes evidenced by the grooving that was seen on the surface. Eventually the remnant coating suddenly disappeared from the surface of the wear track. The sudden removal of the coating occurred when the coating became so thin and indeed was worn through in some positions across the wear track that the rest of the coating was not able to withstand the mechanical stresses imposed on it.

For the TiN coating, only gradual wear of the coating was observed without a sudden failure event, but the applied load in this test was much lower than the higher loads imposed in the Nitron test.

3D FIB-SEM was carried out on the wear tracks on the Nitron and TiN coatings. Figure 13 shows selected frames from a 3D dataset for the Nitron coating sample (video of dataset is available in supplementary information). In these images it can be seen that across much of the wear track although the two-layer coating is not intact, some of the coating still remains across most of the wear track. However, the carbon layer has been removed for most of the width of the wear track. Where the titanium (light contrast) layer has been removed as well there is also some fracture and cracking damage. These results contrast with the top-down observations of wear track where all of the coating seems to have been removed. This is partly because in the imaging used in the top-down analysis it is difficult to distinguish between the titanium layer and the underlying steel substrate.

Figure 14 shows selected frames from the 3D dataset for the TiN coating sample (video of dataset is available in supplementary information). These frames show what seems to be undamaged coating on the right-hand side of the image, with an area where coating has been removed to the left of this, with an area where microstructural mixing has taken place to the left of this. The later images (Figures 14c and 14d) shows that this mixed area also incorporates some elements of the structure of the substrate such as metal carbides. Some separation between different features in this mixed area can be seen, but it was likely that these arise as one element of the material is rolled over another element.

3.2 ROCKWELL TESTING

Typical indentations from Rockwell adhesion tests can be seen in Figure 15. A pattern of cracking can be seen around the indentation for the WC/Co coating (Figure 15a). The cracks form arcs which start perpendicular to the edge of the indentation but then curve around. There are two sets of cracks that have propagated in opposing directions, forming a mesh of intersecting cracks. It should be noted that the WC/Co coating is much thicker, at 150 µm, than the other coatings examined. For this reason, it is not surprising that no sign of delamination is observed for this coating. For the Nitron DLC coating there are also cracks at the edge of the indentation, but there are also small areas where the coating has delaminated and has been removed from the substrate (Figure 15b). The delaminated areas can be seen very

clearly because the substrate (steel) is much more reflective than the coating. The TiN coating also shows cracking (Figure 15c) but there is little sign of delamination.

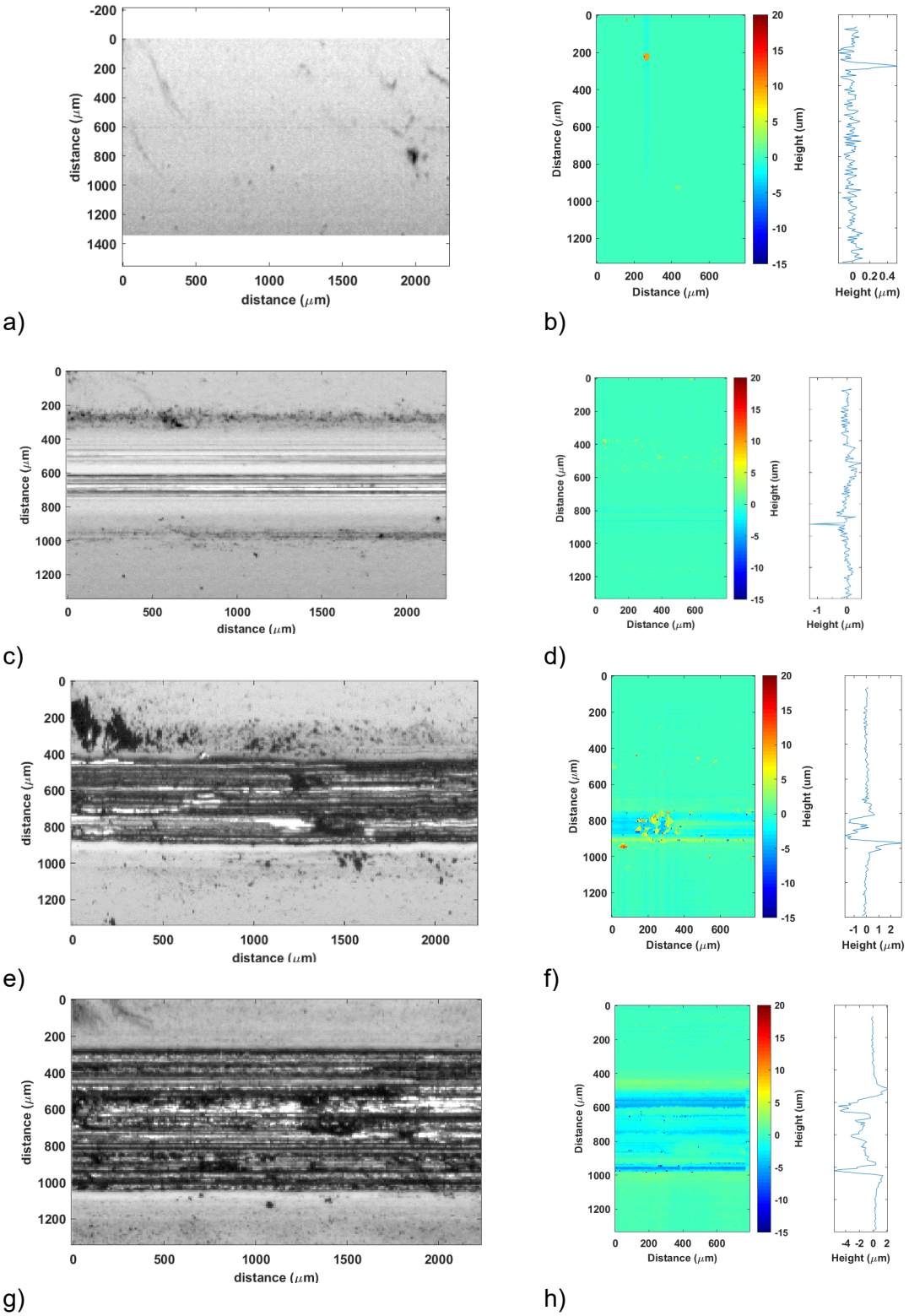

Figure 9: Linescan and multipoint chromatic aberration probe results for Si_3N_4 ball on Nitron disc test, a) linescan image at one rotation, b) height map and profile at 2 rotations, c) linescan image at 1041 rotation, d) height map and profile at 1042 rotations, e) linescan image at 1046 rotations, f) heightmap and profile at 1047 rotations, g) linescan image at 1596 rotations, h) height map and profile at 1597 rotations

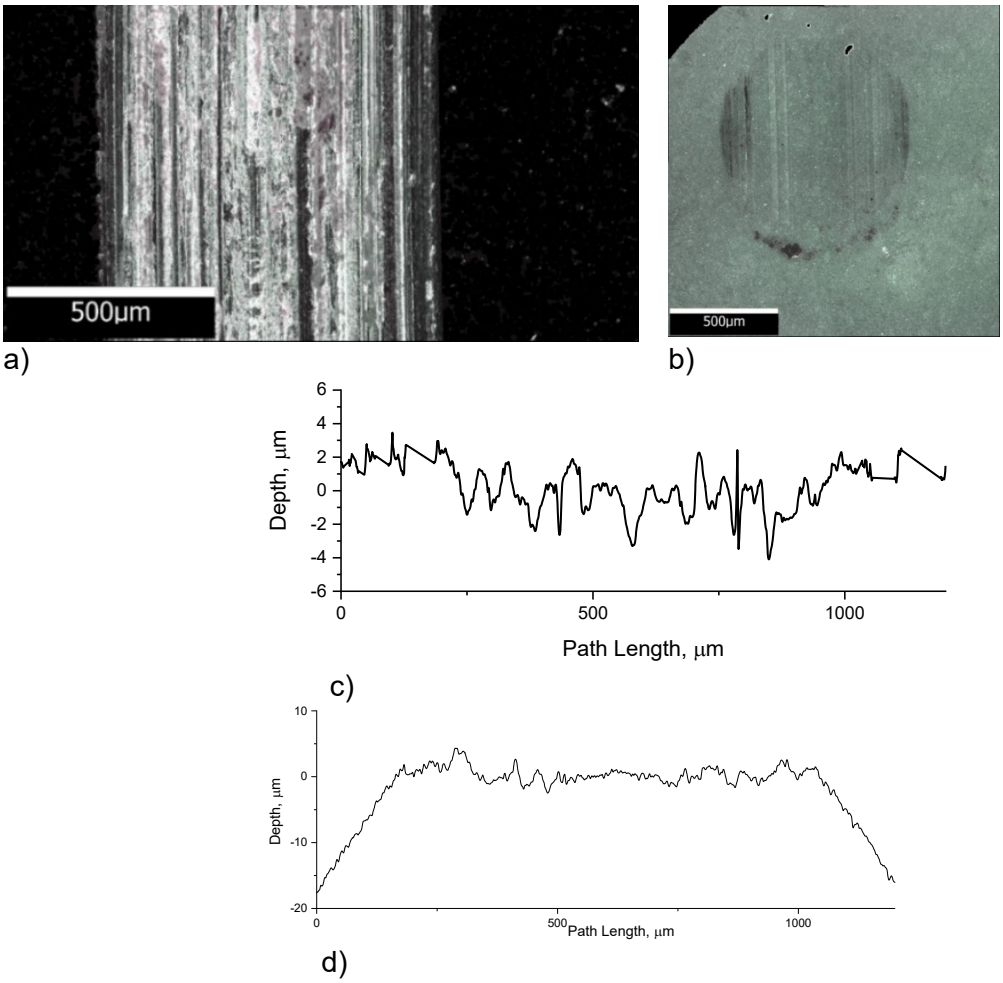

Figure 10: Post-test Alicona analysis of wear surface for Nitron test a) image of wear track, b) image of wear surface on ball, c) profile across wear track, d) profile across ball wear surface (More details in supplementary information, supplementary figures)

SEM images of the indentations and cracks were obtained for the TiN and the Nitron coatings. They are shown in Figures 16 and 17. Figure 16a shows an overall view of the Rockwell indentation in the Nitron coated sample. Figures 16b-16d show small areas of delamination and cracking at the edge of the indentation. There is cracking inside the edge of the indentation as well as outside the edge. Some of the cracks run across the boundary, but others are discontinuous. Figures 16e and 16f show the end of cracks away from the edge of the indentation. These cracks seem to be discontinuous and stepped. It seems likely that some features in the structure of the coating are causing this deviation and stepping in the cracks.

Figure 17a shows an overall view of the indentation in the TiN coated sample. With increase in magnification, there is no significant delamination of the coating at the edge of the indentation, and that irregular cracks again run across the edge of the indentation, but with many cracks starting just outside the indentation edge. Figure 17b and 17e. show some of the crossing cracks noted earlier in the optical micrographs of these indentations (Figure 14). Figure 17d shows a clear example of a crack deviating around a feature in the microstructure of the coating.

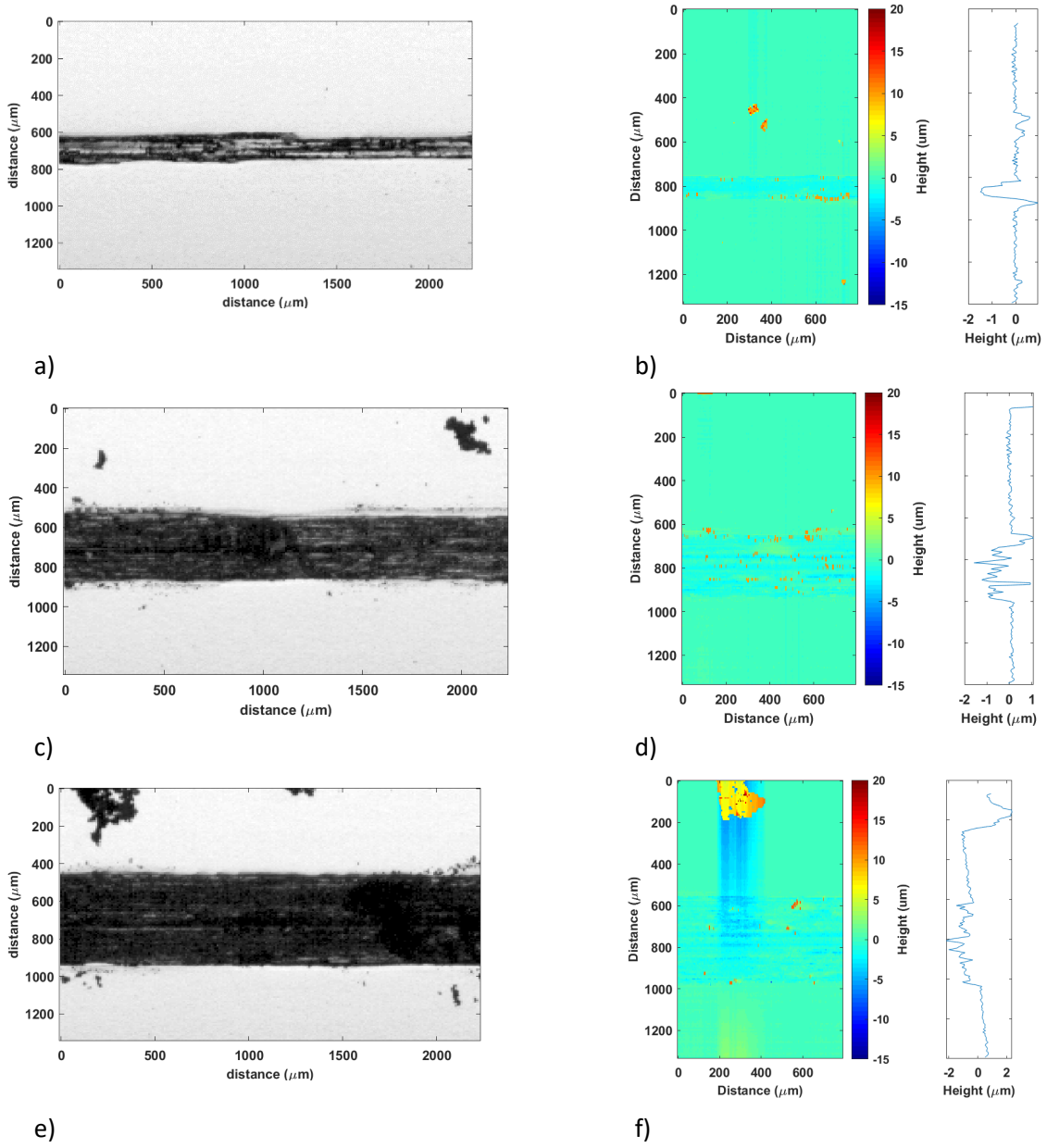

Figure 11: Linescan and multipoint chromatic aberration probe results for Si_3N_4 ball on TiN disc test, a) linescan image at one rotation, b) height map and profile at 2 rotations, c) linescan image at 79 rotations, d) height map and profile at 80 rotations, e) linescan image at 118 rotations, f) heightmap and profile at 119 rotations,

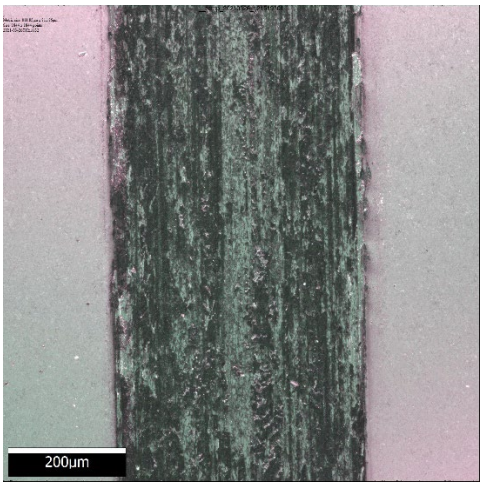

a)

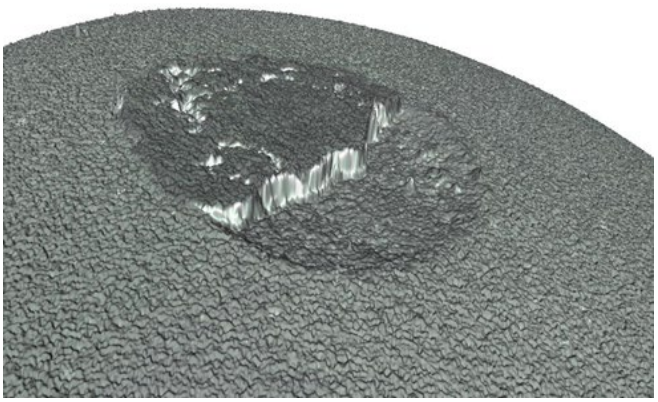

b)

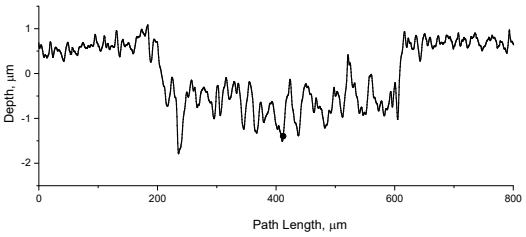

c)

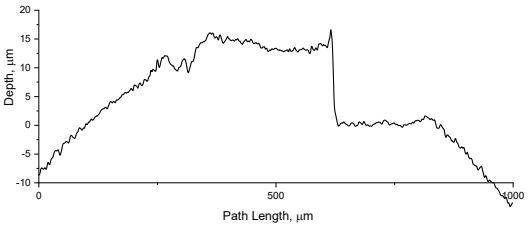

d)

Figure 12, Post-test Alicona analysis of wear surfaces a) image of wear track, b) image of wear surface on ball, c) profile across wear track, d) profile across ball wear surface (More details in supplementary information, supplementary figures)

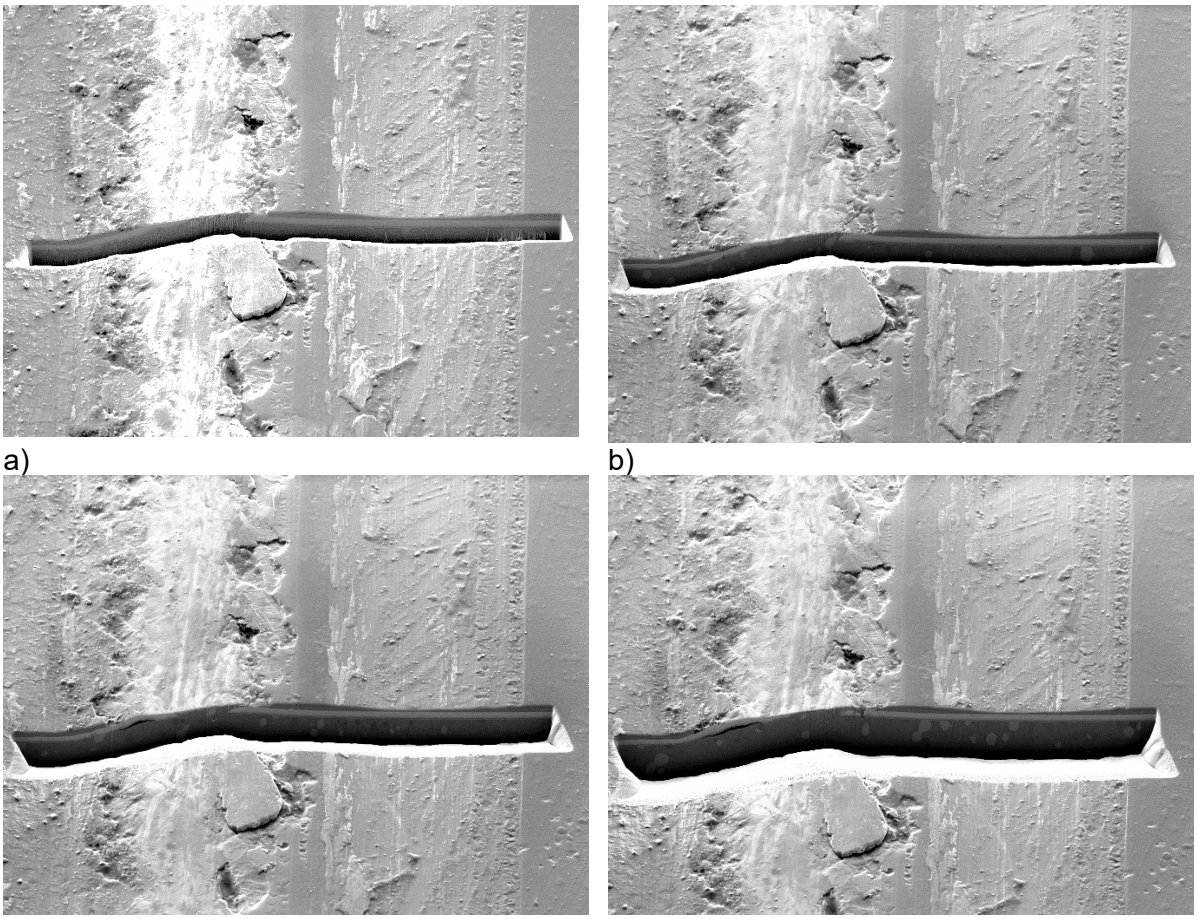

Figure 13: Frames extracted from 3D data set of FIB-SEM analysis of wear track on Nitron coating at a) start of analysis, b) 2 µm from start, c) 4 µm from start, d) 8 µm from start

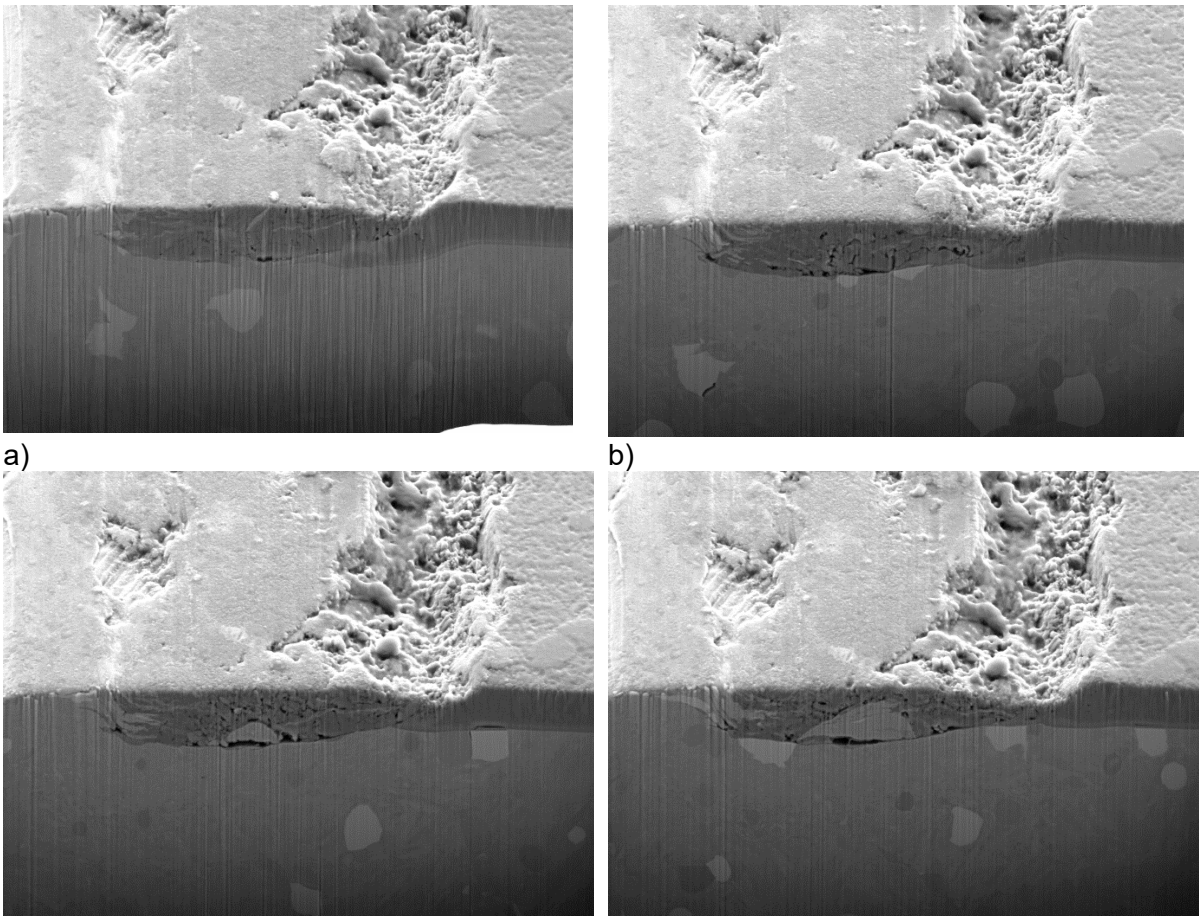

Figure 14: Frames extracted from 3D data set of FIB-SEM analysis of wear track through TiN coating at a) start of analysis, b) 0.9 µm from start, c) 1.8 µm from start, d) 2.7 µm from start

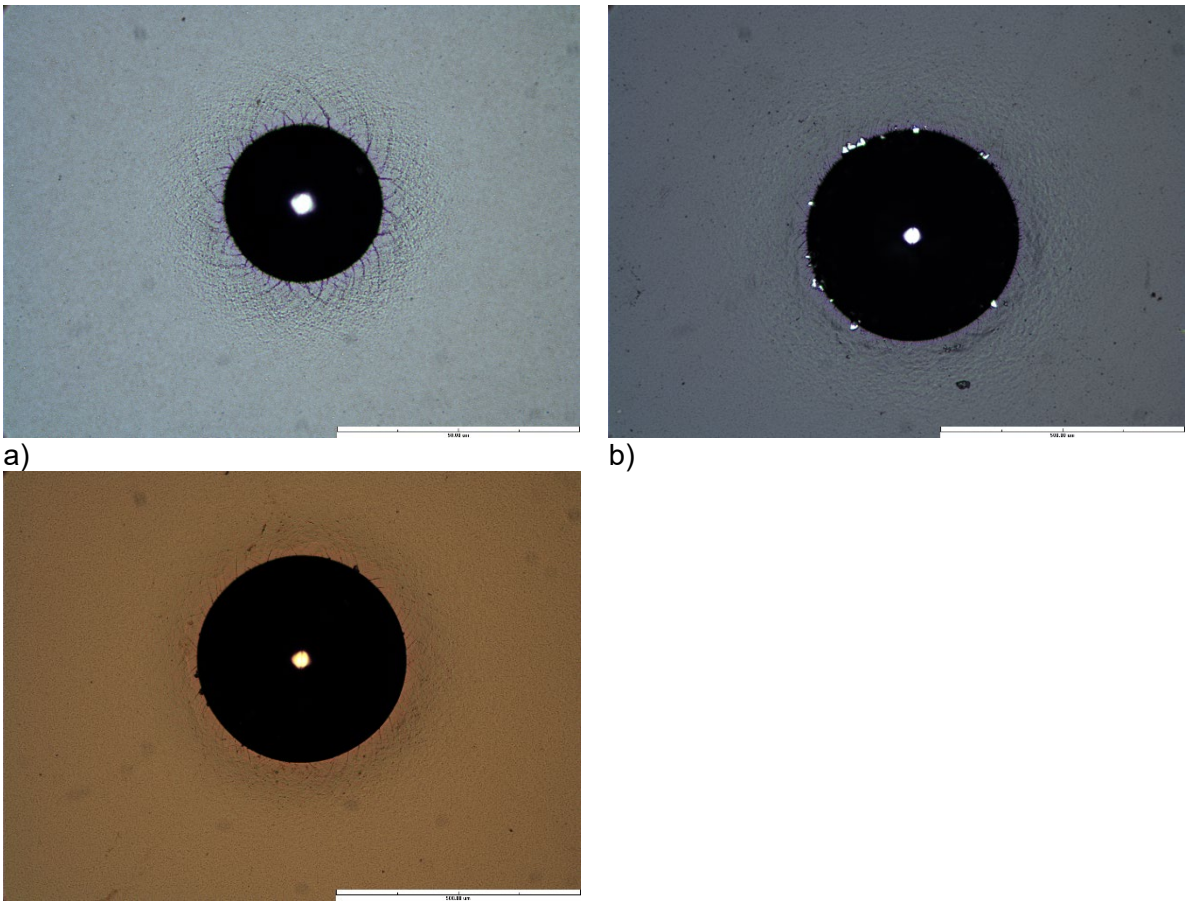

a) b)

c)

Figure 15: Rockwell indentations on 3 different coatings, a) WC/Co, b) Nitron, c) TiN

Figure 18 shows FIB sections through the Nitron coating. Cracks are visible through the coatings and in some cases propagate into the steel substrate. In a couple of cases (Figure 18a) cracks stop at the titanium layer (interpretation of these micrographs can be difficult because of the “curtaining” artefact from FIB which causes additional marks parallel to the surface running from features in the microstructure). In one case a section though one of the cracks that appears stepped on the surface, also stepped in the vertical direction (leftmost crack in Figure 18c).

FIB sections of cracks in the TiN coating are shown in Figure 19. Here there seems to be a lower density of cracks and none of the cracks continue into the substrate.

3.3 SCRATCH TESTING

The results of the critical load evaluation for the TiN and the Nitron coatings are shown in Table 2. Critical load evaluation was not relevant for the WC/Co coating since with the 150 µm coating decohesion and cracking of the same nature were not expected or observed.

For the TiN Lc1 initial cracks were not observed. There was considerable variability in the Lc2 and Lc3 results with Lc2 values ranging from 20.3 N to 51.2 N, and Lc3 results ranging from 23.2 to 61 N. For the Nitron tests Lc1, Lc2 and Lc3 events were all observed. The spread in results for the Nitron tests was less than for the TiN tests.

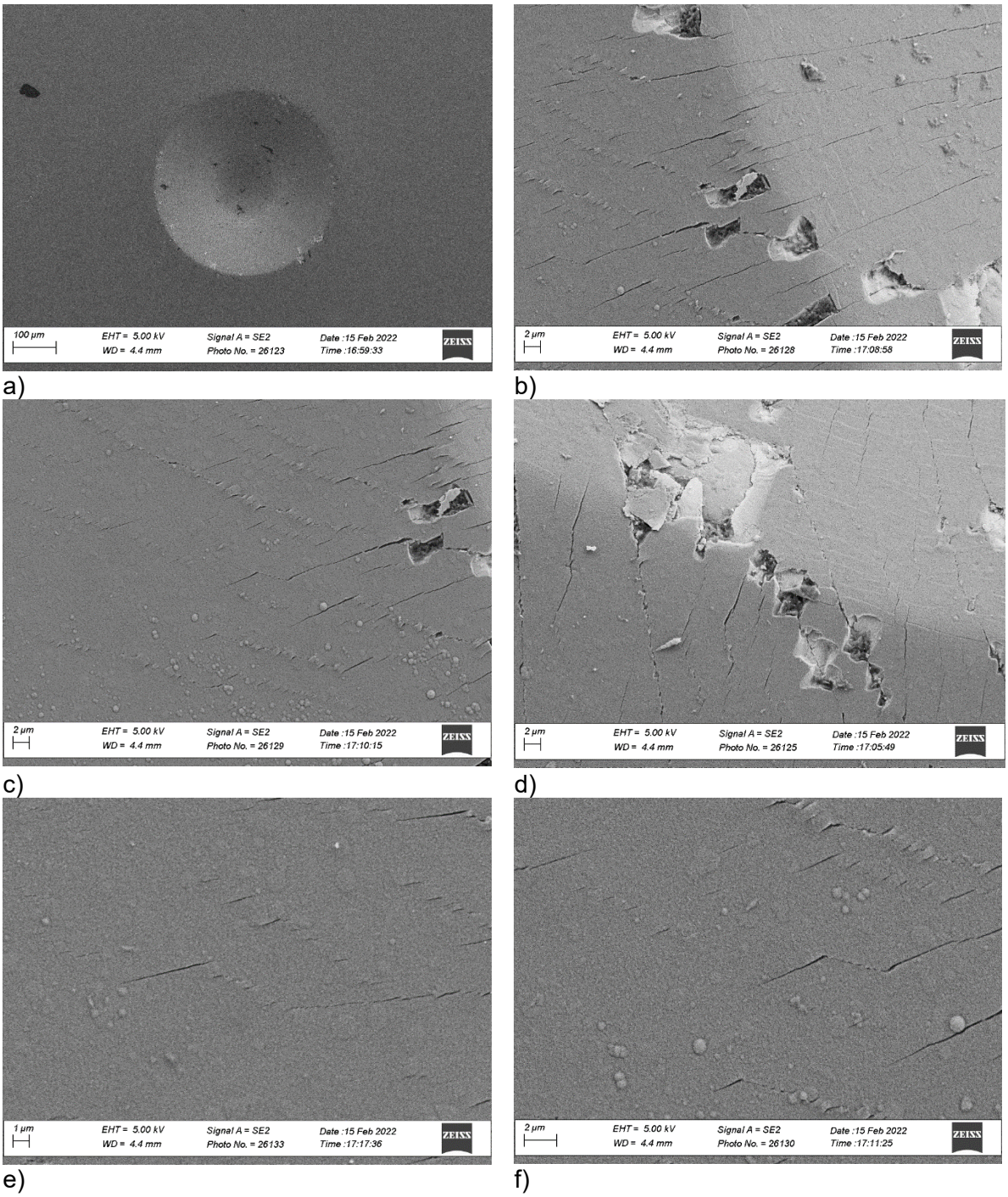

Figure 16: SEM micrographs in sequence of increasing magnification of typical Rockwell crater on Nitron coated tool steel.

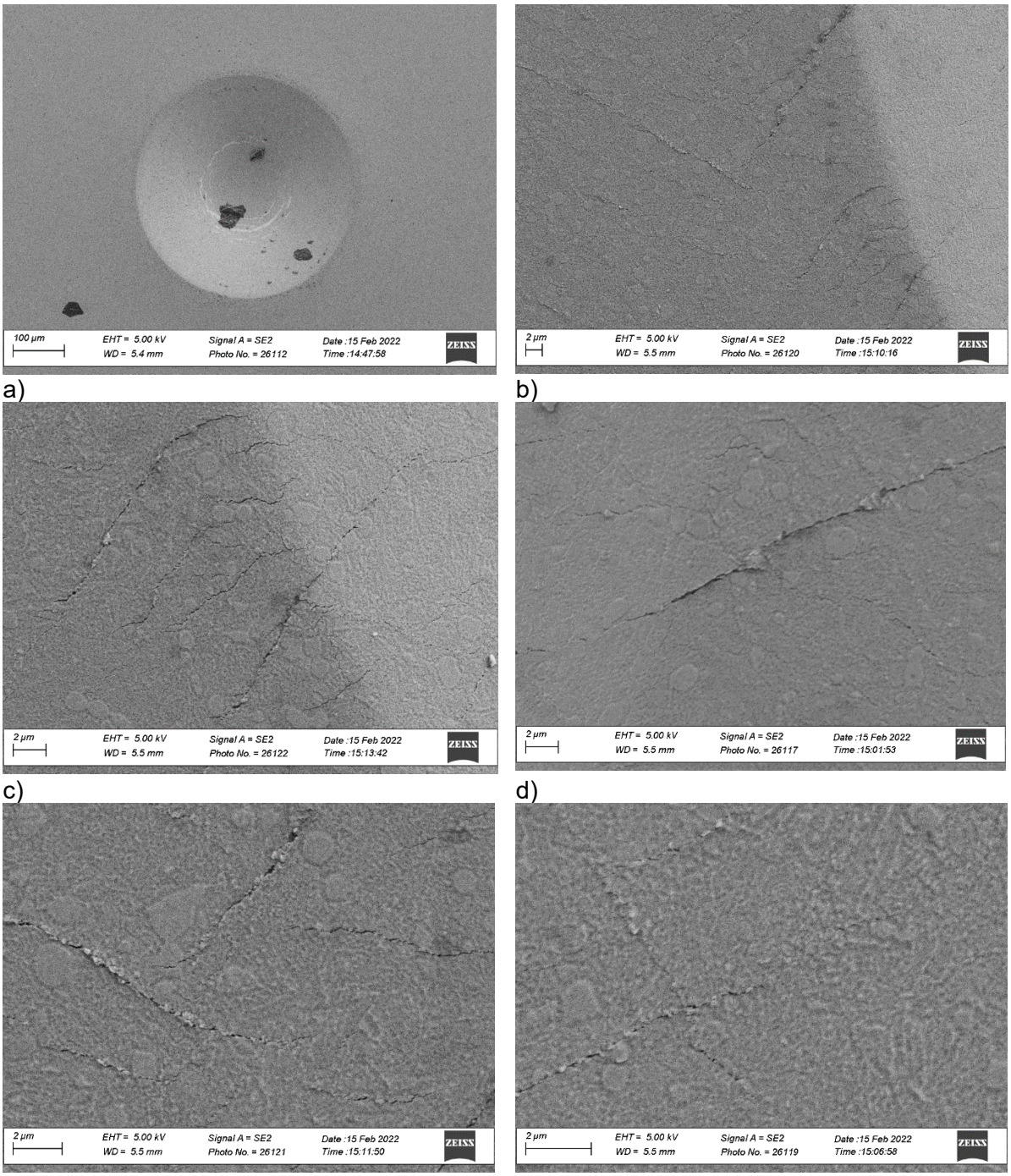

Figure 17: SEM micrographs in sequence of increasing magnification of typical Rockwell crater on TiN coated tool steel.

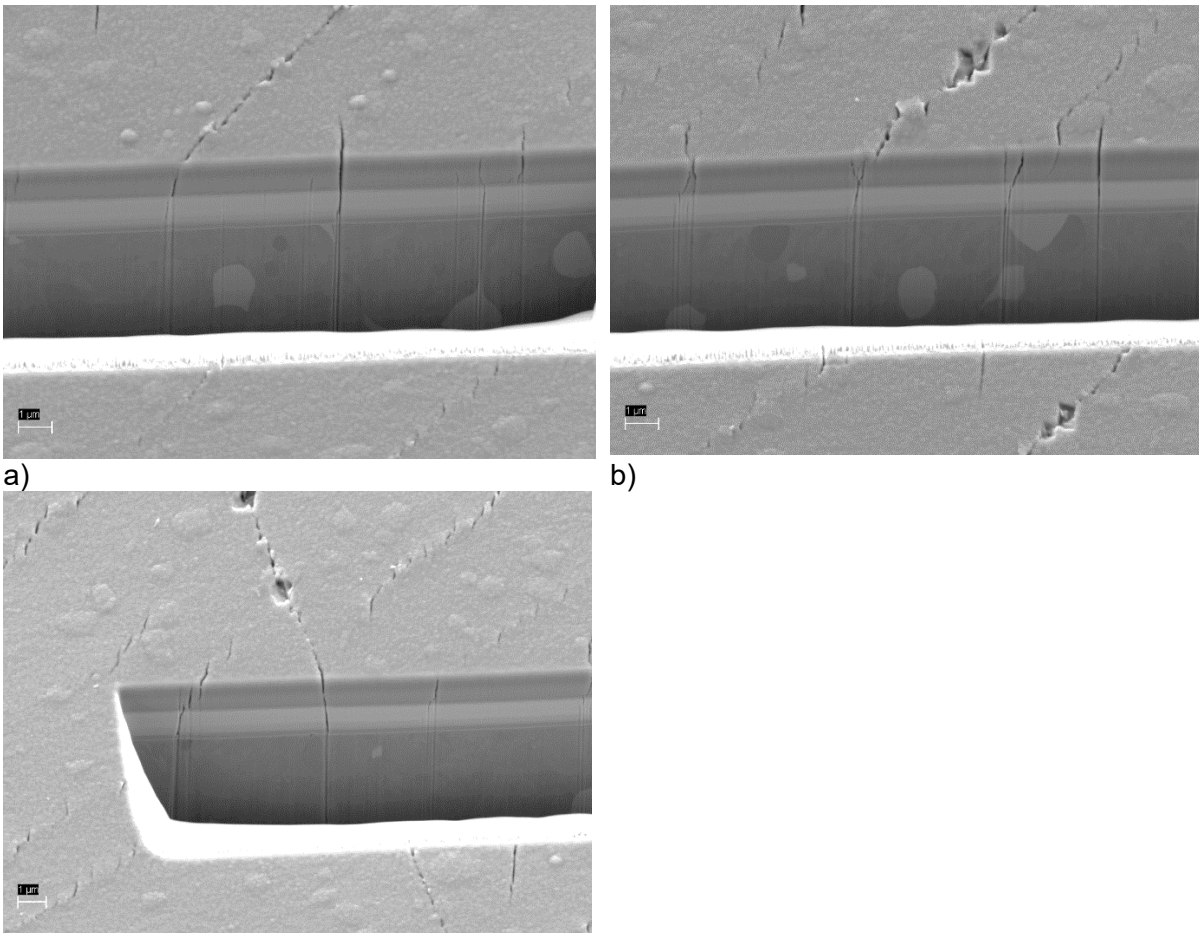

a) b)

c)

Figure 18: FIB cross sections through edge of Nitron Rockwell indentation

Table 2: Critical loads for measurements on TiN and Nitron samples

Material and Scratch Number	Lc1	Lc2	Lc3
TiN 1	-	30.3	35.5
TiN 2	-	51.2	56.3
TiN 3	-	25.0	61.0
TiN 4	-	20.3	23.2
TiN 5	-	20.3	33.4
TiN 6	-	44.0	47.8
Nitron 1	32.8	39.2	45.6
Nitron 2	25.8	25.8	43.0
Nitron 3	26.9	26.9	48.2

Figure 20 shows the friction and acoustic emission results for all the coatings. Sharp increases in friction were observed for all three of the TiN tests and for two of the Nitron tests, suggesting that in these tests the friction had been affected by fracture events in the coatings. In the acoustic emission, the only change that was observed was an increase in the variability of the acoustic emission signal for the TiN coating at about the same value of load as the increase in friction. Only steady increases in friction and acoustic emission were observed for the WC/Co coating.

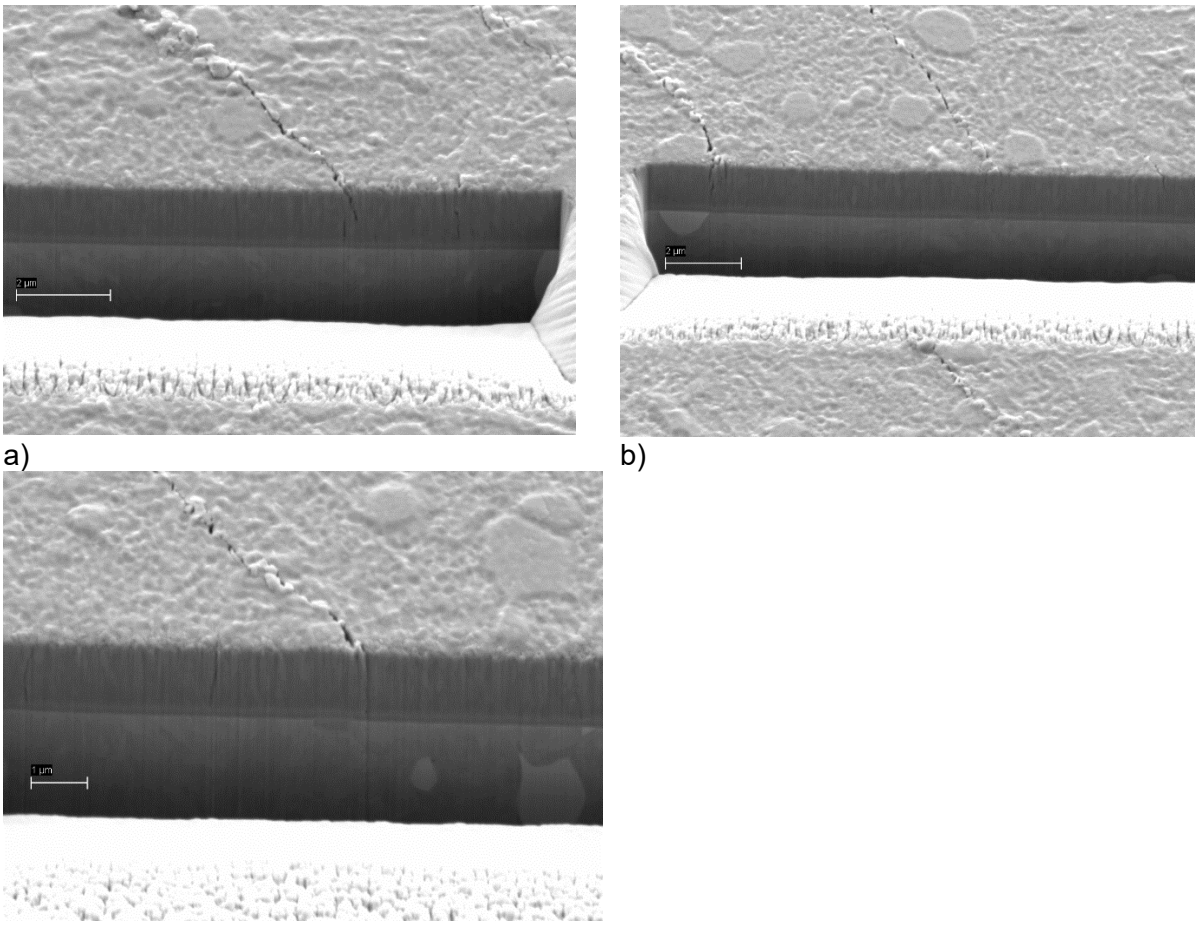

a) b)

c)

Figure 19: FIB cross sections through edge of TiN Rockwell indentation

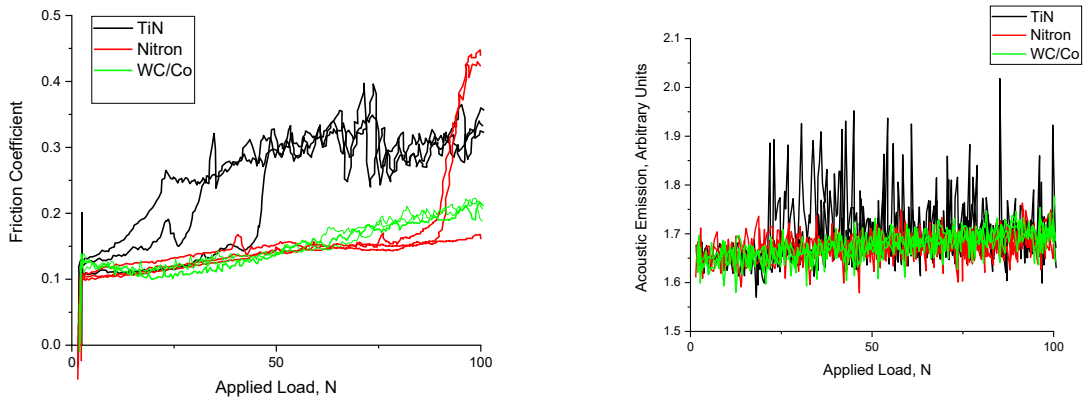

a) b)

Figure 20: a) friction and b) acoustic emission results for three scratches carried out on TiN, Nitron and WC/Co coatings

Figures 21 and 22 show optical microscope images of different failure events on typical Nitron and TiN scratches. These are complimented by SEM images showing different features in scratch tests on the Nitron and TiN coatings in Figures 23 and 24. The Nitron scratch (Figure 23) shows how the coating has apparently delaminated at the edge of the scratch, and also shows the surface layers of the scratch near the edge mixing with different phases evident from the variation in contrast that can be seen.

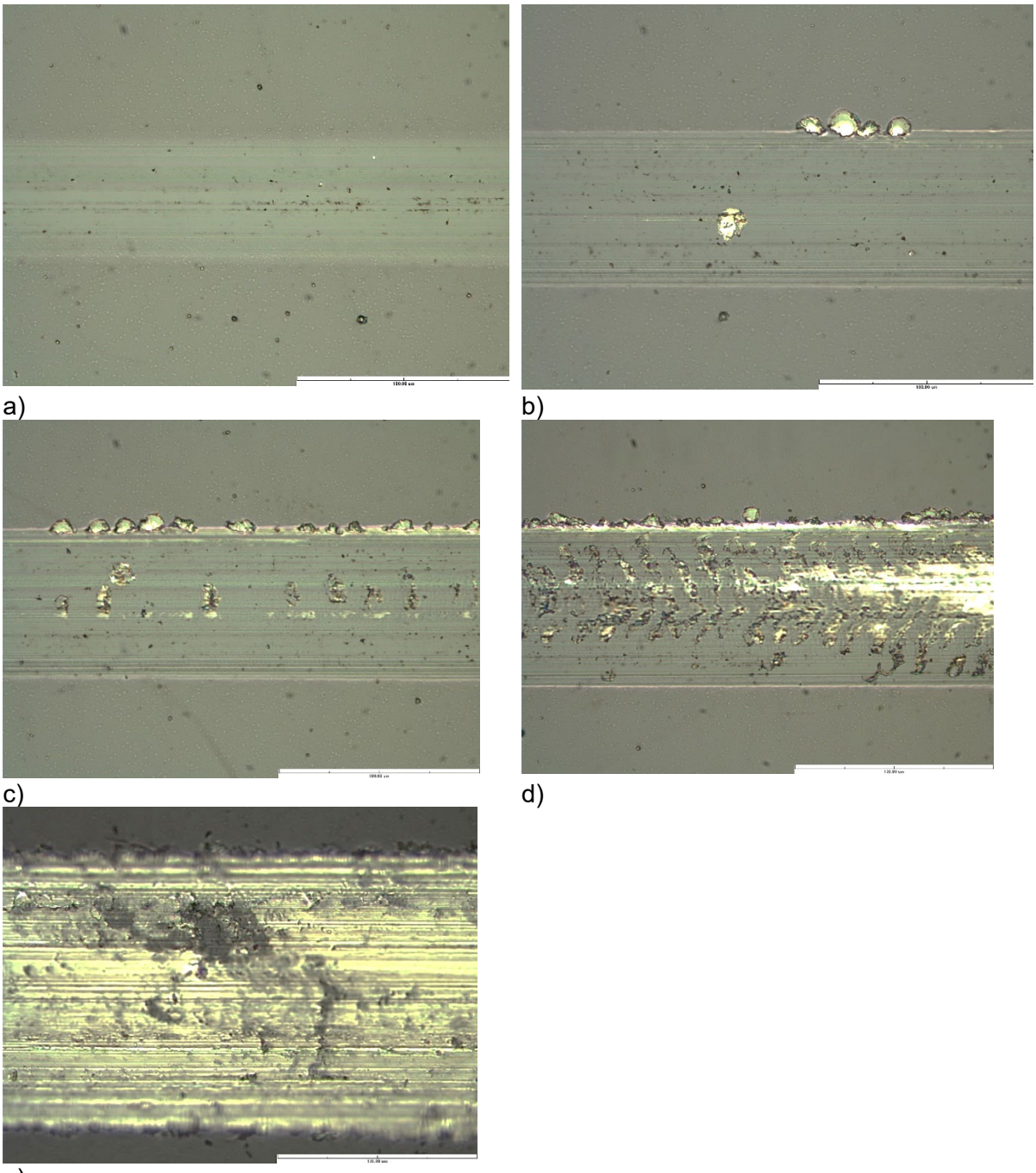

Figure 21: Optical micrographs of a typical scratch on Nitron DLC coating, a) no coating failure at applied load of 17.6 N, b) and c) illustrating Lc1 events at 26.8 and 29.7 N applied load respectively, d) Lc2 events at applied load of 36 N applied load, e) Lc3 (apparent complete loss of coating) at 72.9 N load.

The TiN scratch shows similar features. Figure 24a shows a typical Lc2/Lc3 event showing the failure of the coating. This area is very similar to the area shown in the optical micrograph in Figure 22b. Fragmentation at the edge of the scratch is shown in Figure 24b. In this area the coating has been completely removed from the scratch revealing the characteristic bright contrasting carbides in the substrate. Figures 24 c, d, and e show a more complex area where removal of some coating has occurred, but there also seems to have been some mixing of phases in the surface.

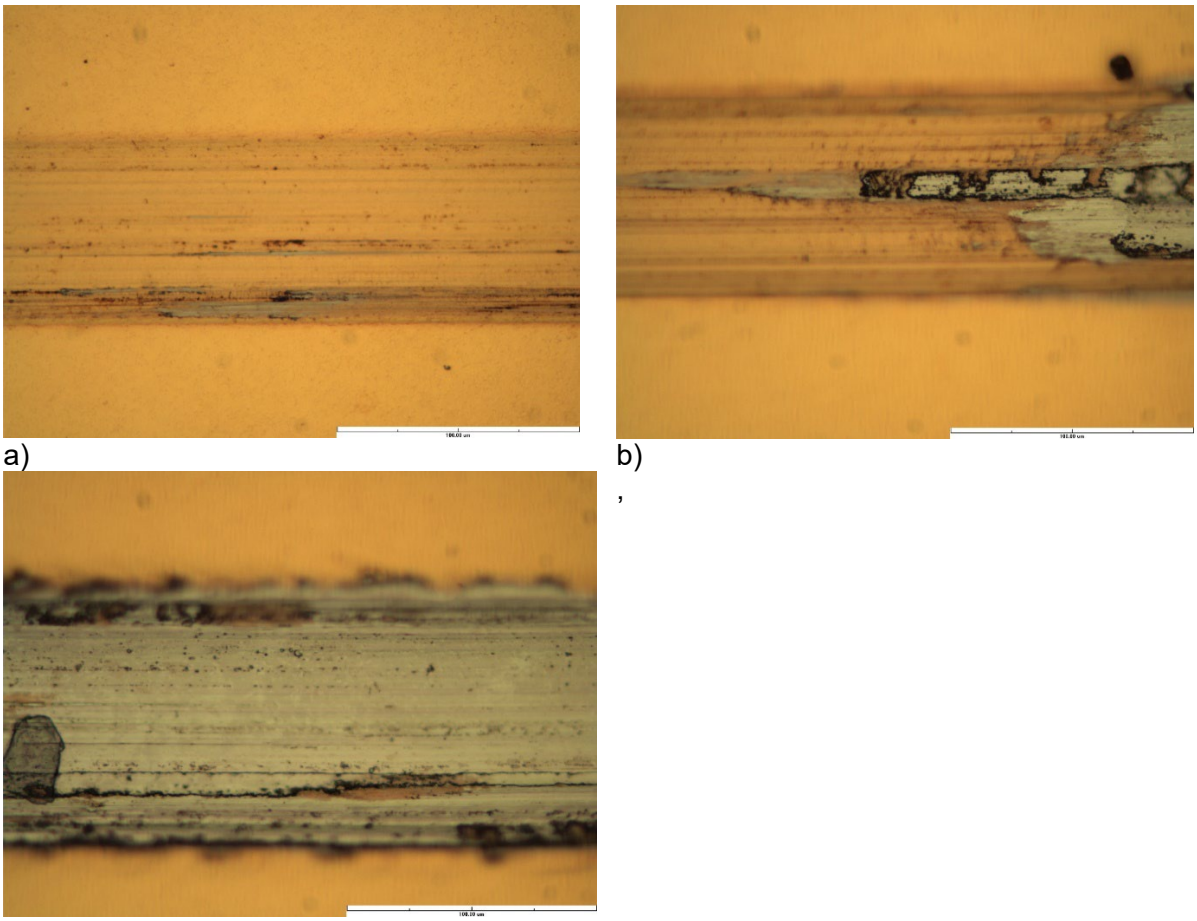

a) b)

,

c)

Figure 22: Optical micrographs of a typical scratch on TiN sample, a) no failure of coating at 30 N applied load, b) Lc2 event at 43.6 N applied load, and c) complete loss of coating at 48.4 N applied load.

Figure 25 shows a sequence of frames from a 3D FIB analysis of the area on the Nitron scratch shown in Figure 23d (The video is in the supplementary information for the report).

Many complex mechanisms are taking place. The failure of the coating is not straight forward. The carbon (dark contrasting) layer has been removed from most of the scratch surface, but the titanium layer (lighter contrast) has separated into different laths that are interspersed with steel laths to form the complex structures seen on the right of the frames. The titanium layer has even lifted and has moved on top of another element of the titanium. Where this takes place cracking in the titanium often occurs under the extreme deformation occurring at this point at the edge of the scratch. In the small delaminated area that is visible in some of the frames, the cross-section through this area shows that it is the carbon layer that has been mostly but not completely removed from this area.

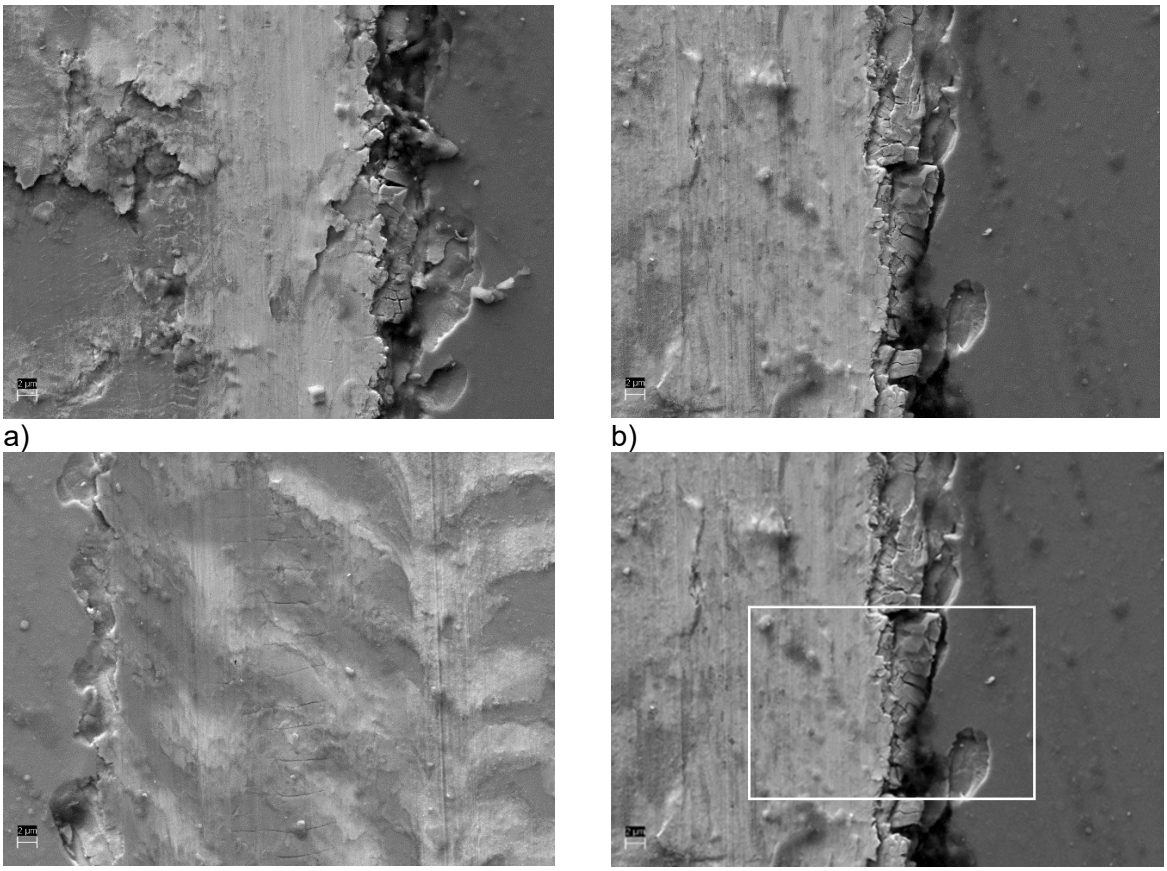

Figure 23: SEM micrographs of scratch on Nitron sample, a) – c) different areas at side of scratch, d) image in b) with rectangle showing area selected for 3D FIB mapping shown in Figure 25.

Figure 26 shows some frames from the 3D FIB analysis of the area of the TiN scratch shown in Figure 24e.

The most noticeable feature that can be seen is that although the top view SEM image shows delamination of coating from the surface, there is still some TiN coating remaining. Over the area which seems to be lifting away from the surface seen in the top view, it is also clear that the coating is suffering from cohesive failure rather than interfacial failure as about half of the coating remains on the surface with a top layer of material held loosely. It can also be seen that many of the surface features that are seen do not propagate into the surface of the scratch.

3.4 ABRASION SIMULATION

Figure 27 shows the results from the abrasion simulation 3D analysis on a scratch carried out by making many repeat passes over the same scratch path. There are two main modes of damage. These are the development of networks of cracking in the top layers of the microstructure under the scratch and the formation of zones of fragmented WC under the scratch. A similar analysis was carried out on a scratch carried out on the same hard metal, but with the surface of the hard metal that was being scratched submerged in HCl.

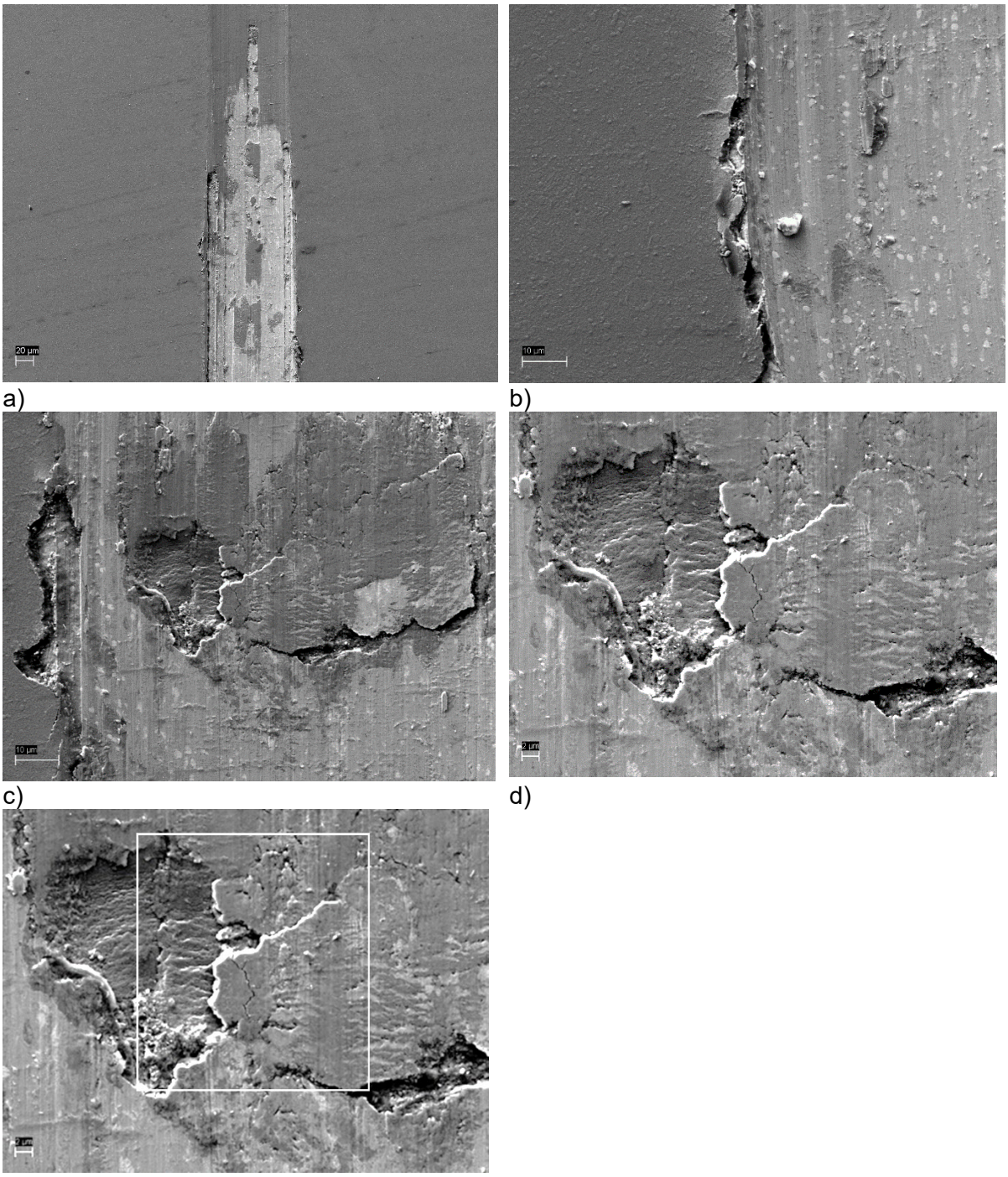

a) b) c) d) e)

Figure 24: SEM micrographs of scratch on TiN coating. a) and b) are different areas at the edge of the scratch. c) and d) are images of an area at the centre of the scratch and e) shows the area selected from the 3D analysis shown in Figure 26.

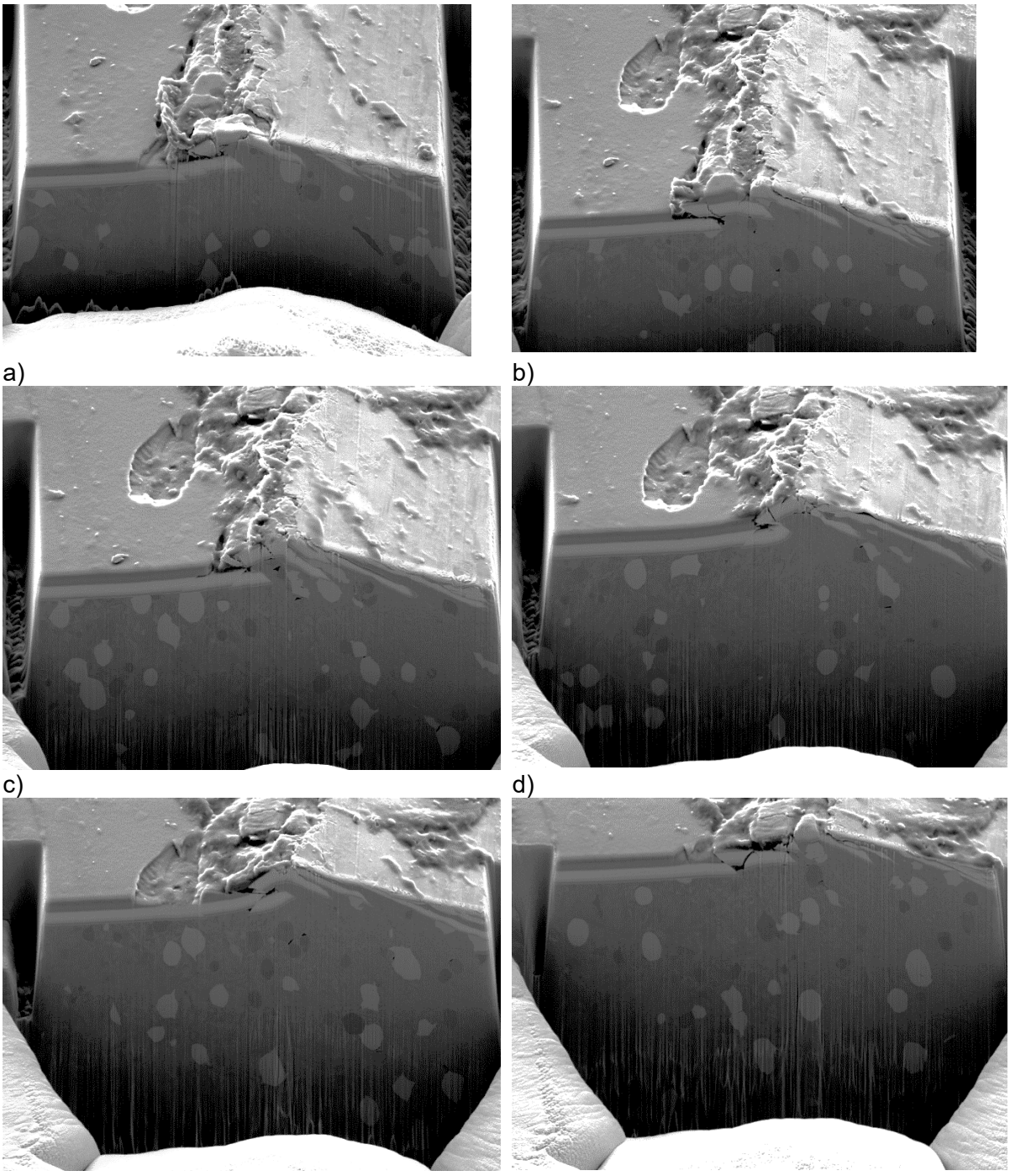

a) b) c) d) e) f)

Figure 25: Frames from 3D dataset of FIB analysis of Nitron scratch from area shown in Figure 23d. Position from start of analysis, a) 288 nm, b) 4320 nm, c) 8640 nm, d) 12960 nm, e) 17280 nm and f) 21600 nm. Sequential frames in the video are separated by 96 nm.

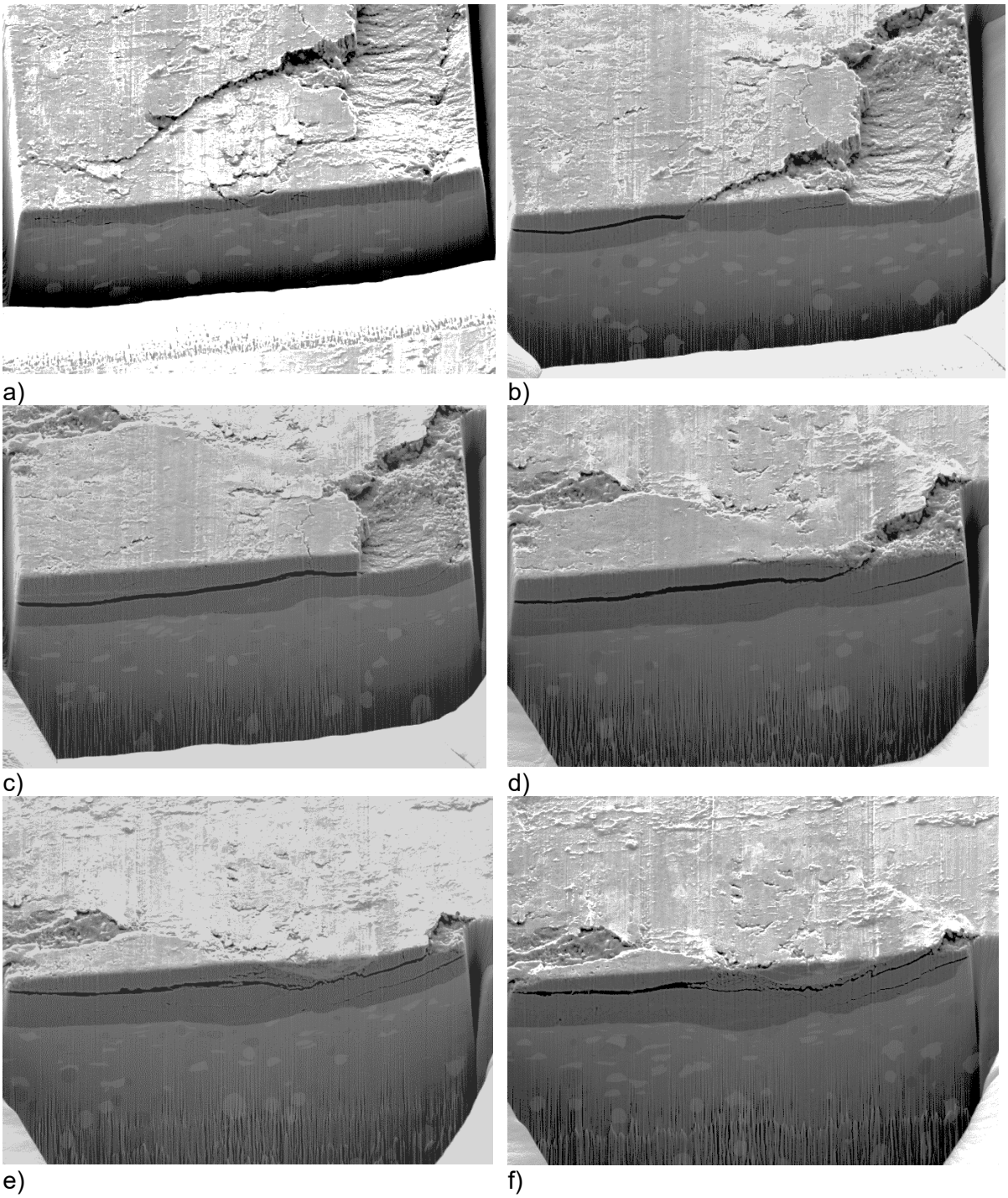

Figure 26: Frames from 3D analysis of 3D data set of FIB analysis of area shown in Figure 24e. Position from start of analysis, a) 105 nm, b) 9835 nm, c) 15995 nm, d) 23030 nm, e) 27510 nm and f) 29085 nm. Sequential frames in the video are separated by 35 nm.

Figure 28 shows the overall results from this analysis. ImageJ was used to examine the 3D data sets. A single frame of the analysis of the dry test is shown in Figure 28a. Here the orange area shows the area identified as cracks. A top-down view of the analysed 3D data sets is shown in Figure 28b for the dry test where the red area is the area of cracks seen from above. Figure 28c shows the analysis for the test carried out in the presence of HCl. The orange area shows the area where cobalt binder phase was removed from the structure of the material, weakening the strength of the material, and the blue area shows the cracking in the surface of the material. Segmentation analysis of the top-down views of the structure showed that the area of cracking in the dry sample was about 44% of the total area, the area of cracking in the

sample exposed with HCl was about 66% and the area of binder phase removal was about 35%.

The resultant decrease in mechanical strength is a major reason why the mass loss for the test carried out in HCl was more than 5 times the mass loss for the test carried out dry (Figure 29).

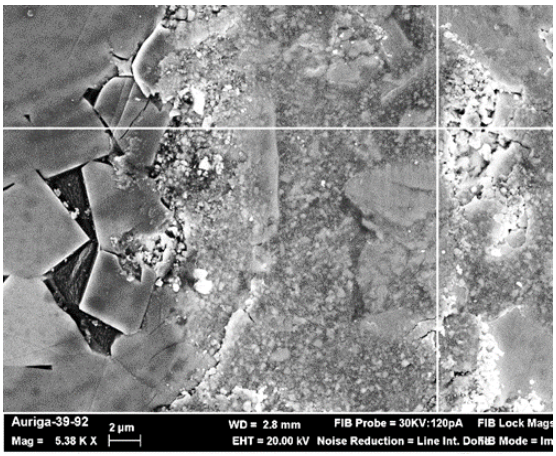

a)

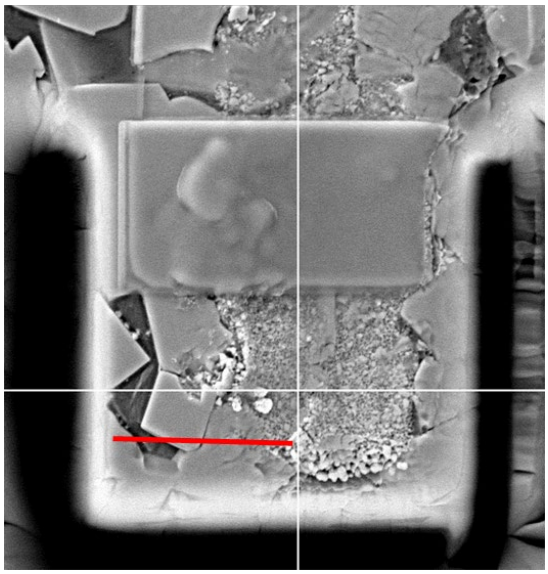

b)

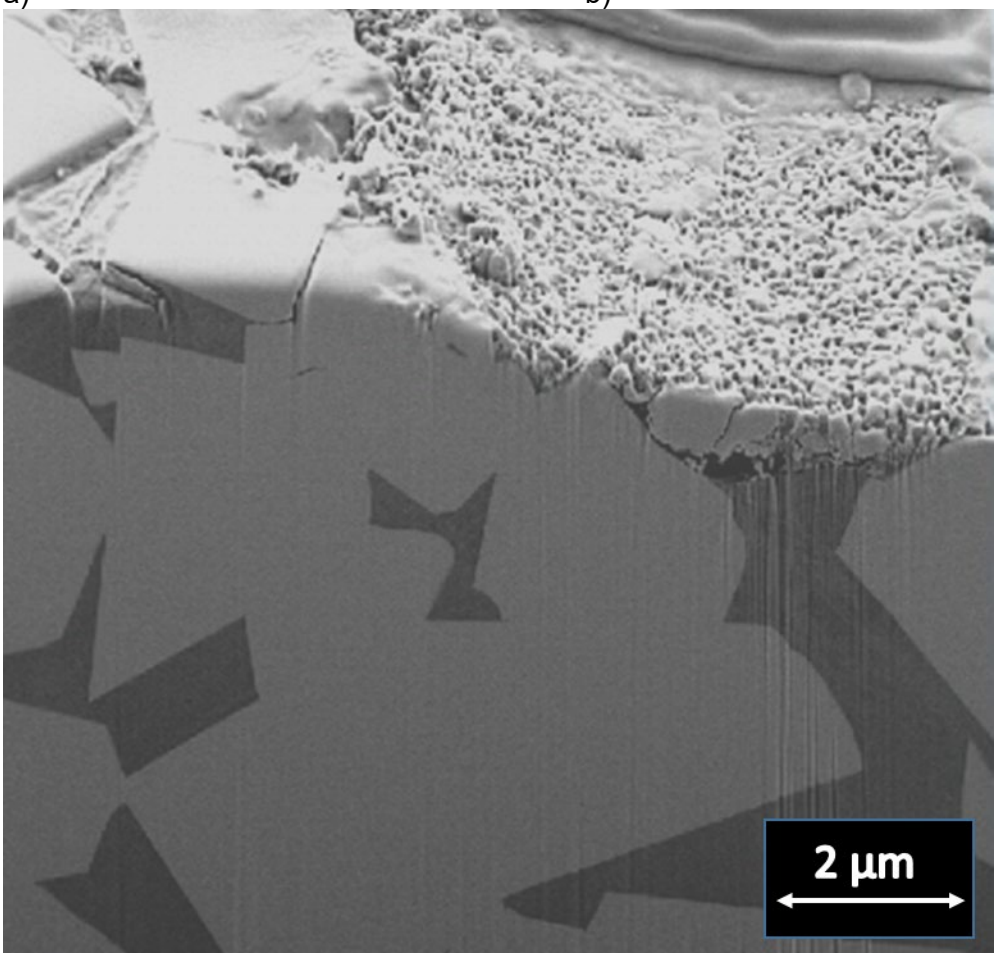

c)

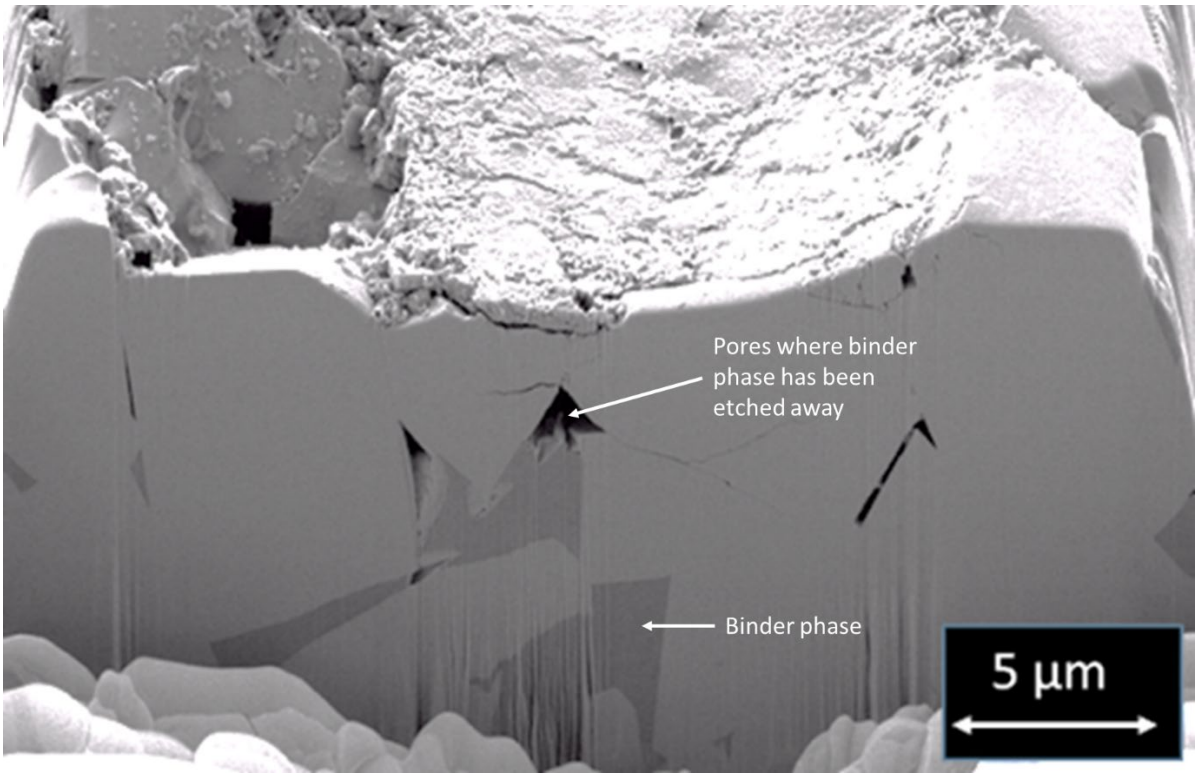

d)

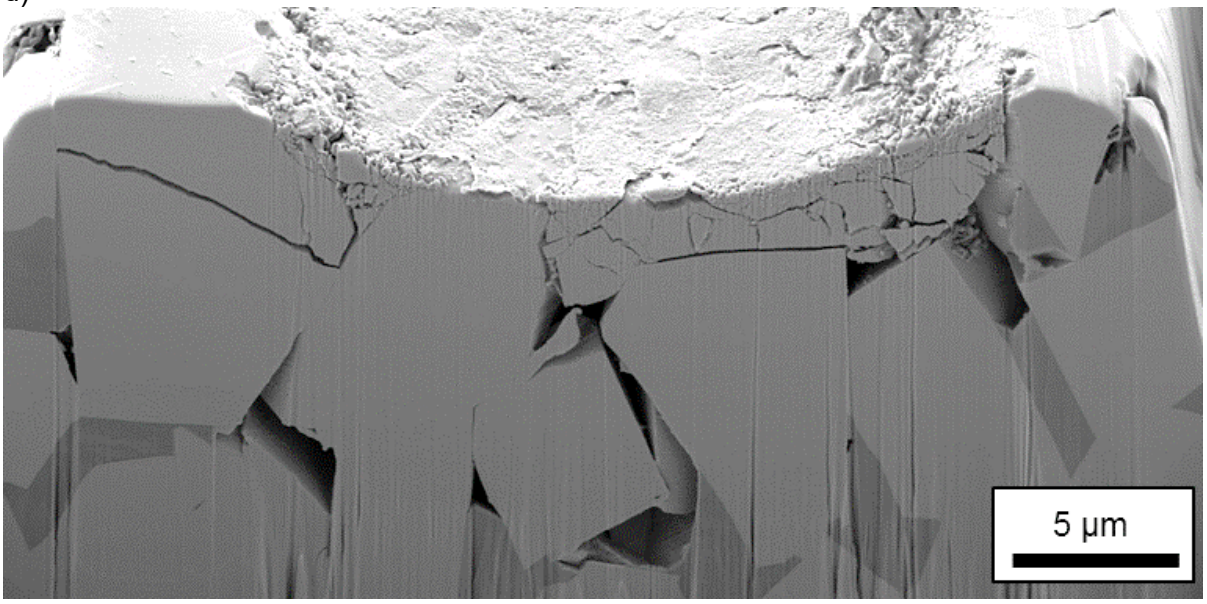

e)

Figure 27: FIB-SEM cross sections through single track scratch experiments, a) surface view of area for examination of mars11E 2000 pass scratch an applied load of 240 mN and a 20 µm indenter, b) preparation of a) for 3D FIB analysis with area protected by Pt deposit and red line indicating position of cross section image presented in c), d) cross section of sample scratched by 200 repeat passes in the presence of HCl on the surface with an applied load of 240 mN and a 20 µm indenter e) image taken about 8 µm further along the dataset. Note that videos from the 3D datasets are in the supplementary information for the report.

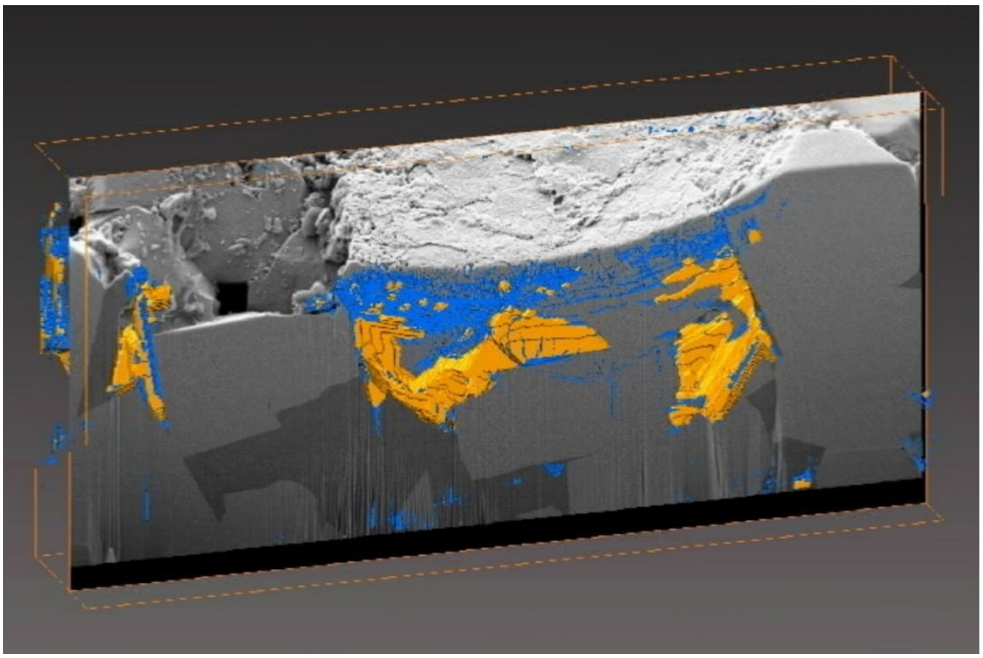

a)

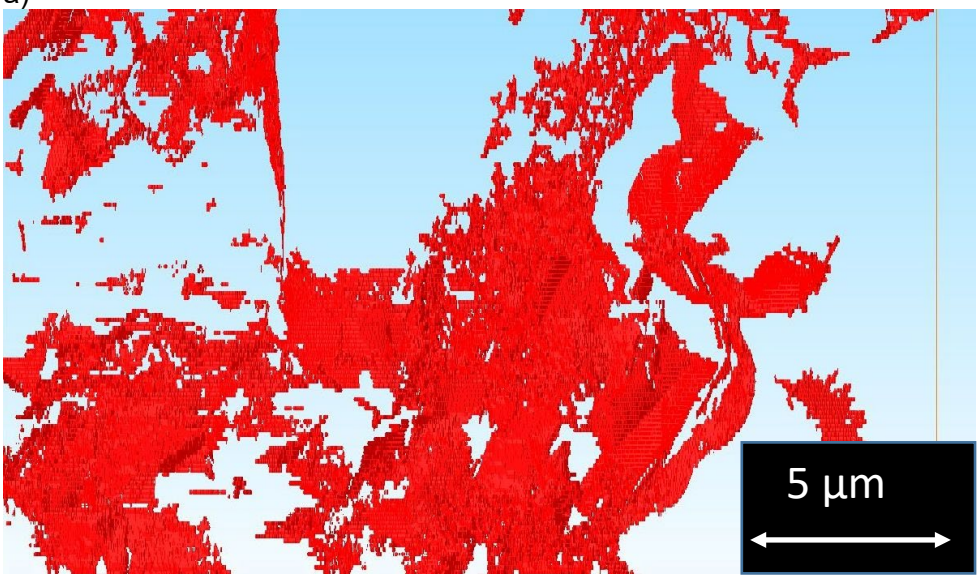

a)

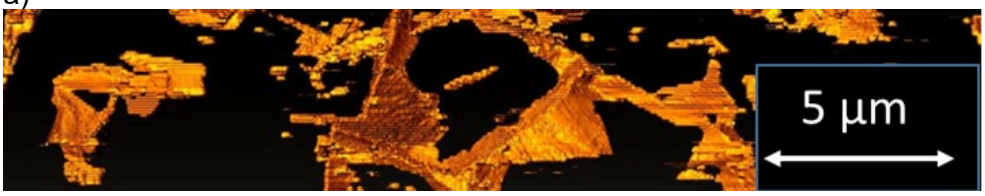

b)

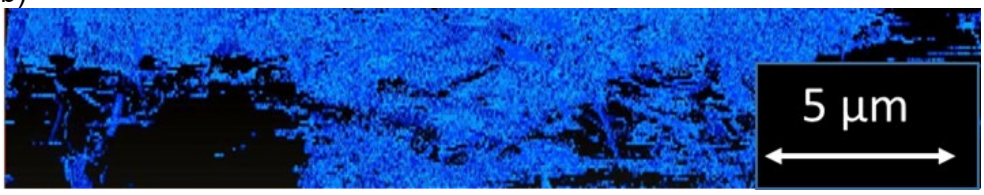

c)

Figure 28: Quantification of cracked area from dry scratched area; view from top, a) dry scratch, b) HCl scratch area where binder phase has been removed, c) area of cracking in HCl exposed ample. Note that videos are in supplementary information.

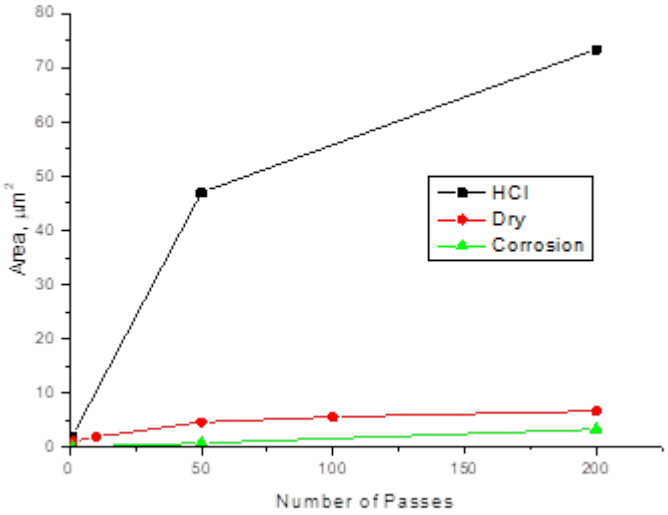

Figure 29: Comparison between area (proportional to volume and mass) lost for repeat pass scratch on 11E hard metal carried out dry and in the presence of HCl.

4 FINAL THOUGHTS

The results gathered in this report illustrate that fracture and cracking processes from localised loading in engineered surfaces are immensely complicated. Even the coating-substrate system means that it is always important to consider the materials properties of all the components in the system when trying to understand the response. Even calculating the stress distribution that occurs in these systems is not simple, although there are commercial software systems available for this purpose [8]. Another factor that is important is the geometric scaling of the coating system and the scale and distribution of the mechanical loading.

It is also clear that in many cases the response of the material can be very variable. Thus, in the scratch testing the variability in the critical load for the TiN coating was very high. This is likely to be because of defects in the coating structure in a coating which has a thickness of only a few micrometres.

The results described in this report clearly show that the use of multiple techniques to provide additional data gives more information and enables a better understanding of the processes that occur. Thus, in the sliding wear testing the use of *in situ* techniques combined with post-test microscopy gives a much more complete picture of materials behaviour than the use of post-test examination techniques by themselves.

In this respect 3D microscopy through FIB-SEM provides an additional dimension. Not only does it give a fuller 3D picture of cracks and fracture processes, but the information that is obtained can change the understanding of what is happening beneath the surface completely. Thus, in the scratch testing of the DLC Nitron coated sample, the deformation processes with the layering of steel and titanium towards the edge of the scratch, and the interfacial failure between the carbon layer and the titanium layer were completely unexpected. Another example was the comparison between the 3D damage caused to the WC/Co material for scratches caried out dry and in the presence of HCl. The analysis of the area of cracking and the area of binder phase that was removed when HCl was present gave an excellent explanation for the synergistic effect of corrosion and wear on material removal that was much greater than either of these aspects by itself.

5 REFERENCES

1. M Gee and T Fry, **A numbers game**, Materials World, November 2021 pp 47-48
2. M Gee, T Kamps, P Woolliams, J Nunn, K Mingard, **In situ real time observation of Tribological behaviour of coatings**, Surface and Coatings Technology, Published electronically, https://doi.org/10.1016/j.surfcoat.2022.128233
3. BS EN ISO 26443:2016 **Fine ceramics (advanced ceramics, advanced technical ceramics) - Rockwell indentation test for evaluation of adhesion of ceramic coatings**.
4. DIN 4856:2018-02, **Carbon-based and other hard coatings – Rockwell penetration test to evaluate the adhesion**, Tech. rep., Beuth-Verlag, Berlin (2018). doi:https://doi.org/10.31030/2795562.
5. N.M.Jennett and S. Owen-Jones, **The Scratch test: Calibration, Verification and the Use of a Certified Reference Material**, NPL Measurement Good Practice Guide No.54
6. C. Pignie, M.G.Gee, J.W.Nunn, H.Jones, A.J.Gant, **Simulation of abrasion to WC/Co hardmetals using a micro-tribology test system**, Wear, 302(2013)1050-1057
7. Mingard, K P; Cox, D C; Jones, H G; Gee, M G, **The use of focused ion beam microscopy for 3D material characterisation**. NPL Measurement Good Practice Guide. 141, 2016
8. Saxonian Institute of Surface Mechanics - SIO (siomec.com)